2013

A computed tomography-based model of the infant hip anatomy for dynamic finite element analysis of hip dysplasia biomechanics

Kyle Snethen
University of Central Florida

A COMPUTED TOMOGRAPHY-BASED MODEL OF THE INFANT HIP ANATOMY FOR DYNAMIC FINITE ELEMENT ANALYSIS OF HIP DYSPLASIA BIOMECHANICS

by

KYLE GEORGE SNETHEN

A thesis submitted in partial fulfillment of the requirements
for the Honors in the Major Program in Mechanical Engineering
in the College of Engineering and Computer Sciences
and in the Burnett Honors College
at the University of Central Florida
Orlando, Florida

Spring Term 2013

Thesis Chair: Alain Kassab

ABSTRACT

Newborns diagnosed with hip dysplasia face severe consequences when treatments fail. The Pavlik harness presents the most common worldwide treatment for correcting this medical hip abnormality in newborns, but becomes increasingly ineffective as subluxation increases. A dynamic finite element analysis on the hip joint would yield results that could provide insight to physicians as to how the Pavlik harness could be optimized to increase its success rate and develop patient-specific treatment plans. The study completes the first step in such an analysis by generating a three-dimensional model of an infant hip joint directly derived from computed tomography imaging in order to accurately represent the anatomical locations of muscle origins and insertions points as well as the unique cartilaginous characteristics of a neonate hip and femur. Such models will further enhance findings on the biomechanics of hip dysplasia that resulted from a preliminary study using computer-aided design to recreate the hip joint. In addition to the models, the orientation of the psoas tendon in a dysplastic hip through full range abduction and flexion was analyzed using a cadaveric dissection. It was determined that the psoas tendon was not an obstruction to reduction when the hip was in flexion so long as the tendon was not adherent to the hip capsule, and therefore can be disregarded in a finite element analysis or dynamic simulation that introduces flexion. The work of this thesis will lay the foundation for complex finite element analyses regarding the biomechanics of hip dysplasia in neonates as well as other hip abnormalities relevant to early child development.

ACKNOWLEDGMENTS

I would like to thank Alain Kassab, Ph.D. for serving as my mentor and guiding me throughout my undergraduate career as well as helping me set and achieve my academic goals. Thank you also for the opportunity to work in the biomechanics lab and pursue my research interests.

I would also like to thank Eduardo Divo, Ph.D. and Manoj Chopra, Ph.D. for completing my thesis committee and supplying supplemental support and guidance. Additionally I would like to recognize my colleague Orlando Ardila for his constant help throughout the course of completion for my thesis.

Finally, I would like to acknowledge Charles Price, M.D. for providing his continual medical expertise and experience to the project and the Orlando Regional Medical Center for making this study possible by supplying numerous CT scans of patients.

TABLE OF CONTENTS

TABLE OF CONTENTS v

LIST OF FIGURES viii

LIST OF TABLES xii

CHAPTER 1 INTRODUCTION 1

1.1 Background 1

1.1.1 Anatomy of the Hip Joint 3

1.1.2 Diagnosis of Hip Dysplasia 6

1.1.3 Hip Dysplasia Treatments 8

1.2 Computer Models Derived From Medical Imaging 10

1.2.1 Computed Tomography – Based Finite Element Models 11

1.2.2 Musculoskeletal Models from Magnetic Resonance Imaging 16

CHAPTER 2 CT-BASED ANATOMICAL MODELING 18

2.1 Generating an Accurate Three-dimensional Pelvis 18

2.2 Development of a Full Femur Three-dimensional Model 23

CHAPTER 3 COMPUTER-AIDED PHYSIOLOGICAL ALTERATIONS 25

3.1 Hip Model Alterations 25

3.1.1 Scaling the Generated Hip model 25

3.1.2 Modifying the Pubis and Ischium 28

3.2 Femur Model Alterations 32

3.2.1 Scaling of the Full Femur Model 32

3.2.2 Segmentation of the Scaled Femur 39

CHAPTER 4 MECHANICAL PROPERTIES 45

4.1 Background 45

4.2 Literature Review 46

4.3 Discussion 47

CHAPTER 5 ORIENTATION OF THE ILIOPSOAS TENDON 51

5.1 Background 51

5.2 Healthy (Non-Dysplastic) Hips 53

5.2.1 0^o Abduction & 0^o Flexion 53

5.2.2 45^o Abduction & 0^o Flexion 55

5.2.3 0^o Abduction & 15-20^o Flexion 56

5.2.4 45^o Abduction & 15-20^o Flexion 56

5.3 Completely Dislocated Hips 57

5.3.1 0^o Abduction & 0^o Flexion 57

5.3.2 0^o Abduction & 90^o Flexion 59

5.3.3 0^o Abduction & $>90^o$ Flexion 60

5.3.4 50^o Abduction & 90^o Flexion 60

5.4 Discussion 61

CHAPTER 6 DISCUSSION 63

6.1 Improvements on Preliminary Studies 63

6.2 A Complete Finite Element Model 65

6.3 Additional Studies 68

CHAPTER 7 CONCLUSIONS 71

LIST OF REFERENCES 74

LIST OF FIGURES

Figure 1.1 Regions of the pelvis bone [5] 3

Figure 1.2 Ossification centers of the pelvis region in newborn infants [6] 4

Figure 1.3 Muscles of the hip joint [7] 5

Figure 1.4 The Barlow (left) and the Ortolani (right) manuevers [8] 6

Figure 1.5 Ultrasound images of a dysplastic (left) and normal hip (right) [9] 7

Figure 1.6 Graf classifications for hip dysplasia in infants [10] 8

Figure 1.7 The Pavlik harness [11] 9

Figure 1.8 Finite Element model of the left side of the pelvis [15] 13

Figure 1.9 Boundary conditions for symmetric, one-sided analysis of the pelvis [15] 13

Figure 1.10 Healthy (left) and dysplastic (right) hip joints [16] 14

Figure 1.11 Healthy (L) and Dysplastic (R) hip joint finite element models [16] 15

Figure 1.12 Finite element model with muscles represented as stiff cables [16] 15

Figure 1.13 3D surface models of bones and muscles derived from MR images [17] 17

Figure 2.1 CT scans of 6-mo.-old (left) and 14-yr.-old (right) diagnosed with hip dysplasia 19

Figure 2.2 Mimics software interface for 6-month-old patient image set; Top (T), Bottom (B), Posterior (P), Anterior (A), Right (R), and Left (L) 20

Figure 2.3 Three-dimensional rendering of the bone present in the 6-month-old patient using Mimics software 21

Figure 2.4 Mimics software interface for 14-year-old patient image set 22

Figure 2.5 Three-dimensional rendering of the 14-year-old anatomy 22

Figure 2.6 CT scan of Visible Human Project image set 23

Figure 2.7 Three-dimensional adult full femur computer model 24

Figure 3.1 Unscaled 3-Matic model of 14-year-old patient with healthy hips 26

Figure 3.2 Side-by-side comparison of the 6-mo.-old model (left) to the 14-yr.-old model (right) 26

Figure 3.3 Superposition of scaled 14-year-old and 6-month-old pelvis. (i) Inferior view, (ii) Superior view, (iii) Front view 28

Figure 3.4 Planes defined to segment the pubis and ischium 29

Figure 3.5 Final segmented pubis and ischium of 14-year-old model 30

Figure 3.6 Superior (left) and inferior (right) view of the adjusted ischium and pubis 31

Figure 3.7 3-Matic superposition of the 6-month-old model and scaled 14-year-old model 31

Figure 3.8 Side-by-side comparison of scaled 14-year-old pelvis with 6-month-old pelvis 32

Figure 3.9 Comparison of scaled 14-year-old partial femur and the Visible Human model 33

Figure 3.10 Pelvis height measurement 34

Figure 3.11 Femoral length measurement 35

Figure 3.12 Superposition of scaled adult femur with the already scaled 14-year-old femur 37

Figure 3.13 Femoral head diameter as a function of age, modified from [6] 38

Figure 3.14 Acetabular shape as a function of age, modified from [6] 38

Figure 3.15 Pelvic radiograph of 6-month-old girl [19] 40

Figure 3.16 Femur postnatal development [20] 40

Figure 3.17 Cortical bone thickness measurements using CT data 42

Figure 3.18 Three-dimensional infant femur model (i) complete view and (ii) cross-sectional view with distinguished cartilage regions 43

Figure 3.19 Final scaled 3-Matic pelvis and femur models representing a 10-week-old infant... 44

Figure 4.1 How equilibrium modulus of articular cartilage changes with age [29] 48

Figure 5.1 Iliopsoas tendon orientation in 0^o abduction and 0^o flexion of a healthy hip 54

Figure 5.2 Computerized model of the iliopsoas tendon positioning during 0^o abduction & 0^o flexion of a healthy hip 54

Figure 5.3 Iliopsoas tendon orientation in 45^o abduction and 0^o flexion of a healthy hip 55

Figure 5.4 Computerized model of iliopsoas tendon positioning during 45^o abduction & 0^o flexion of a healthy hip 56

Figure 5.5 Iliopsoas tendon orientation in 0^o abduction and 0^o flexion of a dysplastic hip 58

Figure 5.6 Computerized model of iliopsoas tendon orientation during 0^o abduction & 0^o flexion of a dysplastic hip 58

Figure 5.7 Iliopsoas tendon orientation in 0^o abduction and 90^o flexion of a dysplastic hip..... 59

Figure 5.8 Computerized model of iliopsoas tendon positioning during 0^o abduction & 90^o flexion of a dysplastic hip 60

Figure 5.9 Computer model of iliopsoas tendon positioning during 50^o abduction & 90^o flexion of a dysplastic hip 61

Figure 6.1 Simplified SolidWorks model of an infant hip joint [33]..... 64

Figure 6.2 Volume meshes of an infant pelvis and femur assembled in Abaqus 66

Figure 6.3 Muscle lines of actions applied to hip model 67

Figure 6.4 Hip model in the hyperflexion configuration 69

Figure 6.5 Superior view of femur computer models with varying AV angles..... 70

LIST OF TABLES

Table 3.1 Summary of Pelvic Height Measurements [6] 35

Table 3.2 Cortical bone thickness measurements of Visible Human femur 41

Table 4.1 Cortical and cancellous material properties in the hip joint 46

CHAPTER 1
INTRODUCTION

1.1 Background

Hip dysplasia refers to a medical condition where the femoral head rests displaced from its physiological location in the acetabulum. When present at birth, as commonly the case, the condition is diagnosed as Congenital Hip Dysplasia or Congenital Hip Dislocation. The term is synonymous with Developmental Hip Dysplasia (DHD) or Developmental Hip Dislocation because this is a condition that develops in the late stages of pregnancy or after delivery. Thus it is not a true congenital defect but involves late stages of fetal development that are influenced by environment and genetic predispositions. The cause to the multifactorial condition remains unknown; however, large fetal size and breech delivery as well as family genetics have all been attributed to increasing the probability of the disease.

The Pavlik harness poses the standard worldwide treatment for this natal disorder that affects 2-3 out of 1000 full term newborns [1]. The harness has been in use since the 1950s, but continues to fail in 15% of cases [2]. Natvity statistics report over 2.4 million births in the United States in 2006 and similar numbers for 2008 [3]. Based on these trends one can predict that 7,000 babies each year will be affected by this abnormality of which 1,600 will fail treatment, and thus face serious developmental consequences.

The severity of the displacement varies from case to case. In the least severe case, the physiological alignment is only slightly off resulting in no aesthetic abnormalities, and may not cause any symptoms until the patient has entered adulthood. Most commonly, the acetabulum presents too shallow a cavity for the femoral head to rest correctly in, and thus irregular pressure

exerts onto the acetabular lip leading to pain and possible bone and cartilage damage. The most severe case occurs when the femoral head dislocates completely outside of the acetabulum which can lead to the formation of an irregular acetabulum and subsequent hip immobility.

Upon birth, the neonate acetabulum consists primarily of cartilage allowing the femoral head to slip freely in and out of the cup-shaped cavity; however, this cartilage ossifies as the infant matures over the first postnatal year creating a structural hip socket. If hip dysplasia remains untreated early in child development, the acetabulum can ossify into an irregular position requiring reconstructive surgery to fix, or a lifelong abnormality in walking and even complete failure of the affected socket joint. Untreated patients typically require full hip replacements by the age of 50-years-old and the disorder is responsible for as many as 76% of osteoarthritis cases constituting a deep understanding of the mechanics of this treatment as a crucial matter [4].

To gain a more in-depth perspective on how the muscles of the hip joint interact with the Pavlik harness in reducing the femoral head back into its correct anatomical location within the acetabulum, finite element models of an infant pelvis and femurs derived from computer tomography (CT) image sets will be generated allowing for a dynamic analysis simulating the reduction of a displaced femoral head when oriented in the configuration constrained by the Pavlik harness. From this study, it will be clear which direction the muscle resultant loads should be vectored by the Pavlik harness in order to reinforce the natural reduction path as well as provide details to the reduction mechanism necessary for correction. Such analysis will also lay the foundation for further studies involving the interacting forces and torques involved with hip reduction and how the magnitudes of these forces vary through full range abduction and flexion.

This would provide an avenue for physicians to develop patient-specific treatment plans, and thus increase the effectiveness of the Pavlik harness or introduce new treatment methods.

1.1.1 Anatomy of the Hip Joint

The hip joint functions essentially as a ball (the femoral head) and a socket (the acetabulum). The spheroidal joint comprises two main bones, the femur and the pelvis, which articulate at the femoral head and acetabulum respectively. When the femoral head becomes dislodged from the acetabulum, as observed with hip dysplasia, the head of the femur typically resides posteriorly and superiorly of the acetabulum. The regions of the pelvis bone are portrayed in Figure 1.1. The pelvis is constructed of two pelvic bones which are oriented symmetrically on the left and right about the mid-sagittal plane with the sacrum (1) and coccyx joining the two posteriorly and the symphysis pubis (5) anteriorly. Furthermore, each pelvis bone consists of the ilium (2), ischium (3), and pubis (4).

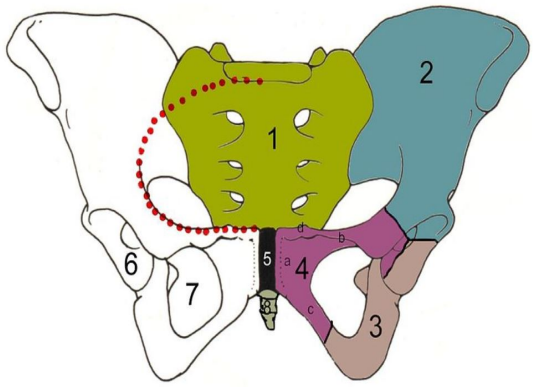

Figure 1.1 Regions of the pelvis bone [5]

At birth, the pelvis and femur have yet to completely ossify, and are thus composed of various ossification nuclei embedded in cartilage throughout the structure as depicted in Figure 1.2 [6]. In Figure 1.2, the noted regions are as follows: ossification center of pelvic cartilage (A), ossified superior ramus of pubic bone (B), non-ossified inferior ramus (C), ilium (D), obturator foramen (E), and sacrum (F). From the onset of birth, these ossification nuclei begin to propagate throughout the cartilaginous regions until a complete bony structure is complete. These cartilaginous characteristics of the infant hip play a significant role in the outcome of hip dysplasia treatments. If detected early, hip dislocation can be corrected before the acetabulum is able to ossify preventing the need for invasive surgeries, while as the infant matures the probability of treating the condition without such procedures diminishes significantly. Due to the natural ossification process of the pelvis and femur along with the goal for noninvasive reduction, it is imperative that hip dysplasia is diagnosed at an early age and corrective action implemented hastily.

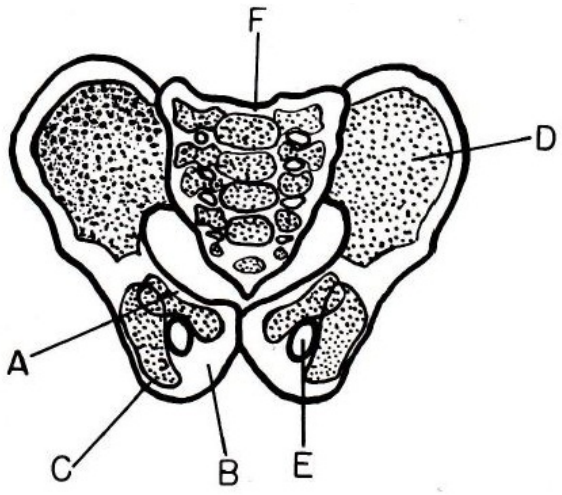

Figure 1.2 Ossification centers of the pelvis region in newborn infants [6]

The muscles and ligaments surrounding the hip joint provide the stability required for normal mobility. The adductor brevis, adductor longus, adductor magnus, gracilis, and pectineus muscles (Figure 1.3) combine to be the key contributors for hip reduction as they naturally adduct the femur when in a passive state. These muscles will be the main focus of this study.

In healthy hips, the joint capsule serves to preserve the integrity and functionality of the ball-and-socket joint preventing the femoral head from sliding out of the acetabulum. The iliofemoral, pubofemoral, and ischiofemoral ligaments are dense, fibrous tissues that make up the joint capsule. The internal teres ligament originates from the center surface of the acetabular cup and attaches onto the femoral head providing supplemental restraint to the positioning of the femoral head. During dislocation, however, this capsule along with the teres ligament are distorted and provide no support to the hip joint, and therefore will be disregarded in this study.

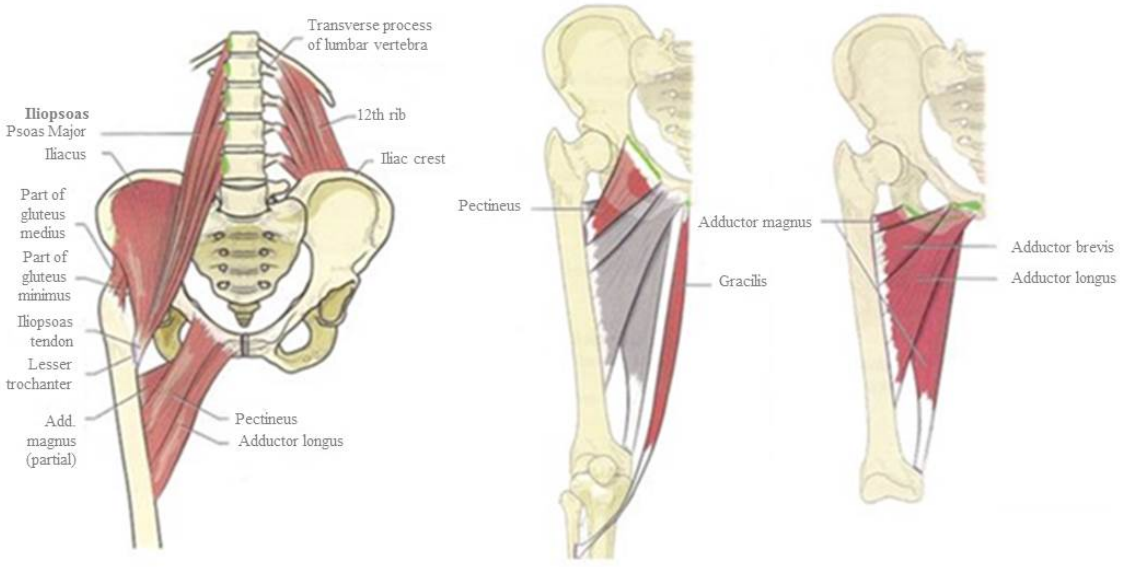

Figure 1.3 Muscles of the hip joint [7]

1.1.2 Diagnosis of Hip Dysplasia

Physical examination performed by a physician at birth introduces the most straight forward means of detecting hip dysplasia. The two established maneuvers for physical examinations are Ortolani and Barlow (Figure 1.4), both of which require the newborn to be in the supine position on his or her back. In the Ortolani technique, the legs are bent at the knee into a 90^{o} orientation with respect to the hip and individually abducted. The Ortolani technique is used to diagnose a fully dislocated hip. A positive test can be distinguished by palpations felt or an audible clunk heard by the physician during the abduction which would indicate the femoral head slipping back into the acetabulum, and thus hip dislocation. The Barlow procedure simply flexes and adducts each leg individually in a manner that draws the leg back over top of the body. This procedure identifies an unstable hip that can be dislocated or subluxated with minor pressure applied to the joint. During the adduction the physician feels if the femoral head slips out of the acetabulum in order to confirm a positive Barlow examination.

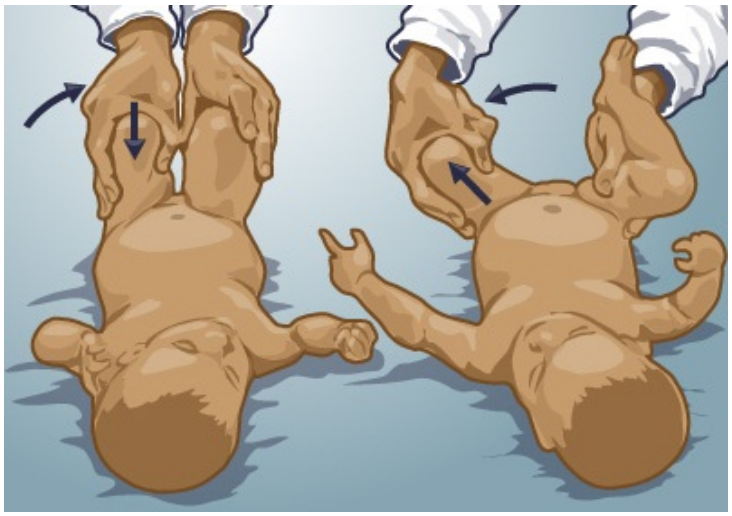

Figure 1.4 The Barlow (left) and the Ortolani (right) manuevers [8]

For an infant under nine months of age, verification of the physical examinations entails observing an ultrasound on the joint (Figure 1.5) [9]. Clarke details the technique and pertinent anatomical landmarks used to detect hip dysplasia using the ultrasound method [9].

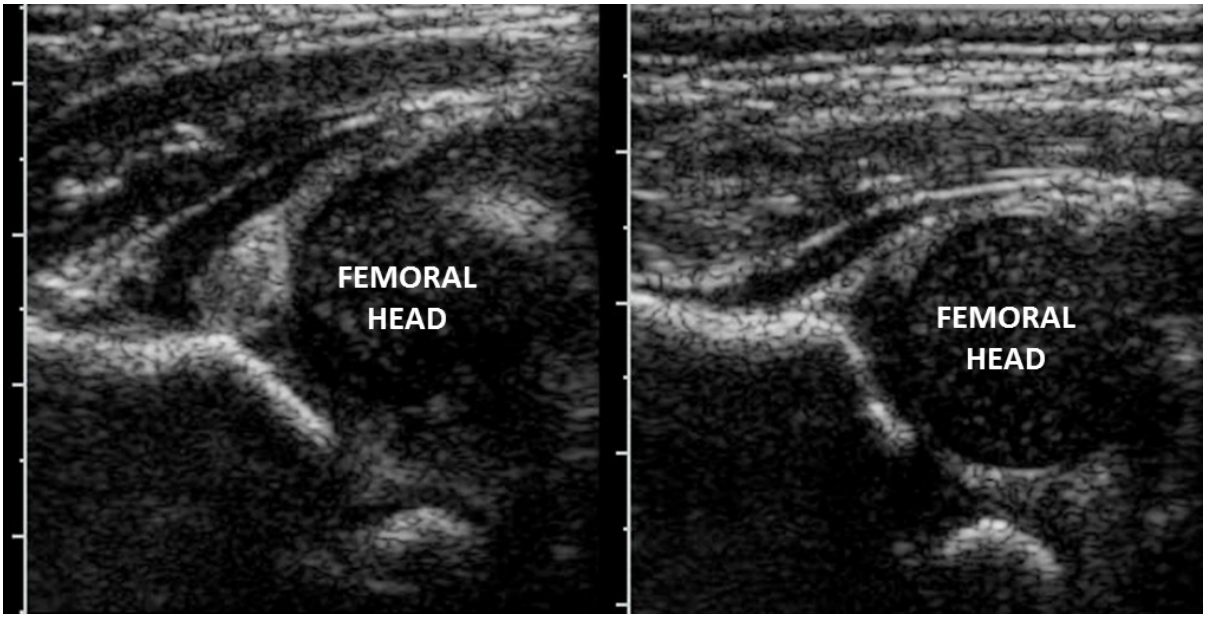

Figure 1.5 Ultrasound images of a dysplastic (left) and normal hip (right) [9]

In the early 1980's, Graf established a means of diagnosing the severity of hip dysplasia using ultrasound. This sonographic screening method not only provided an alternative to the physical examinations previously stated, but also established standardized classifications describing the severity of dysplasia in the patient. Graf developed four benchmarks for diagnosis comprised of Type I, Type II, Type III, and Type IV hip dysplasia which increase in severity (Figure 1.6). A Graf Type I represents a normal infant hip with the femoral head located within a developed acetabular cup. Graf Type II identifies a shallow acetabulum with a rounded rim

leading to a mild state of dysplasia while Graf Type III characterizes subluxation where the femoral head exhibits some displacement due to a very shallow acetabulum. Graf Type IV, the most severe, indicates a flat acetabular roof and hence complete dislocation of the femoral head [10].

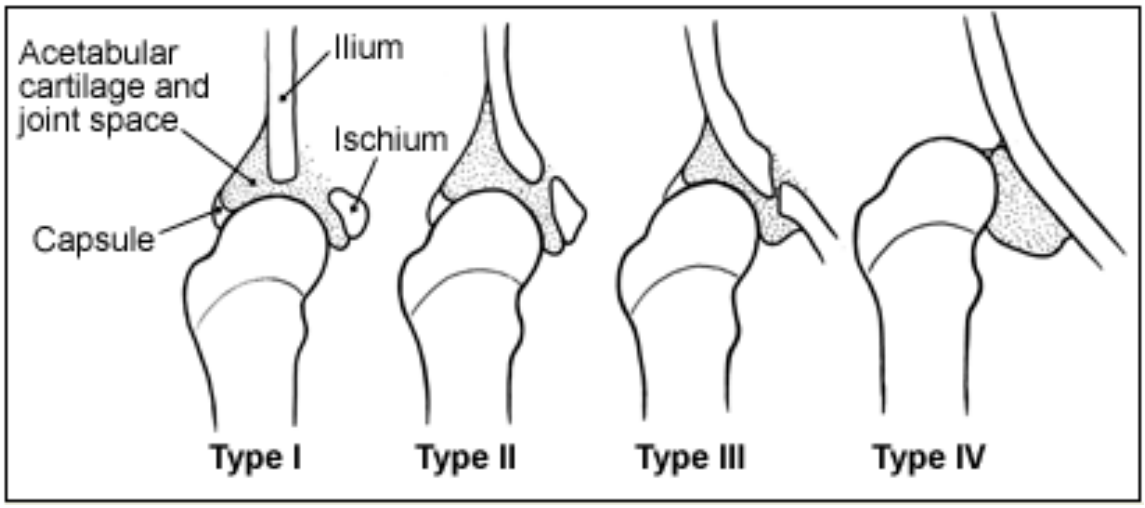

Figure 1.6 Graf classifications for hip dysplasia in infants [10]

1.1.3 Hip Dysplasia Treatments

The Pavlik harness represents the standard of treatment for newborns with hip dysplasia worldwide. The device as shown in Figure 1.7 consists of two shoulder straps (1,2), a chest strap, two back straps (7,8), leg straps(5,6) and stirrups (3,4). This design allows for gradual reduction of the infant hip as the femurs are maintained in an orientation such that the femoral head is vectored towards the acetabulum at all times. Patients wear the harness full-time for a span of 6-12 weeks with the exception for bathing and diaper changes so long as the legs are still kept apart and aimed towards the hip joint. Biweekly check-ups are required to screen for

complications such as femoral nerve palsy and to assess patient progress; the physician adjusts the harness via the straps as needed. If dislocation persists after 4-6 weeks, the treatment is discontinued in order to prevent unnecessary damage to the hip. Physicians recommend treatment using the Pavlik harness for infants between the ages of one month to nine months. The harness fulfills maximum effectiveness when worn immediately after birth, and its rate of success diminishes significantly as the infant matures.

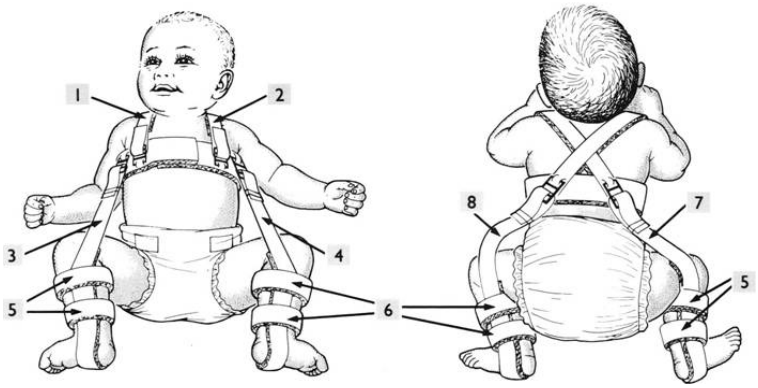

Figure 1.7 The Pavlik harness [11]

Some of the major issues prevalent with the Pavlik harness treatment include nonconcentric reduction of the femoral head with respect to the acetabulum, and avascular necrosis [2]. Additionally, patients face the risk of delayed or incomplete acetabular development, disproportionate hip adductors, femoral nerve palsy, and inferior dislocation [12,13]. As stated previously, failure occurs in 15% of cases, and this failure rate doubles when treatment begins after the patient reaches 3 weeks of age leading to severe consequences [2,14]. Treatment failure rates for the Pavlik Harness also increase with increasing severity of

dislocation. In many cases, failure leads to invasive surgical procedures and complications such as osteoarthritis, avascular necrosis, as well as limited motion of the hip joint. When successful reduction is achieved, however, the probability for re-dislocation is minimal and patients regain normal mobility throughout growth. Therefore, it is clear increasing the success of the Pavlik harness is an urgent matter.

If the Pavlik harness proves ineffective, closed and open reduction procedures are the ensuing steps for hip reduction treatment. In closed reduction, the patient undergoes general anesthesia procedures and the physician manually shifts the femur in a manner that places it back into its normal anatomical position within the acetabulum with only a small incisions being made to release the adductor tendon. Unlike closed reduction, open reduction involves a more invasive technique that requires dissecting the hip joint including incisions on the surrounding tissue and muscles in order to expose the joint to the surgeon so that the femoral head can be realigned within the acetabulum. Following each procedure, a spica cast is worn by the patient to maintain the corrected positioning of the hip and to allow for proper healing. Both open and closed reductions are considered secondary treatments to the Pavlik harness and are typically not performed after the patient reaches 2 years of age. After this age an osteotomy would be necessary.

1.2 Computer Models Derived From Medical Imaging

Due to the advancement in technology, engineers and physicians have been provided a means for accurately analyzing the biomechanics and musculoskeletal interactions of the hip joint. The finite element method (FEM) allows for the discretization of the human anatomy into

an array of adjacent nodes from which various analyses can be performed given the proper mechanical properties and boundary conditions. The initial step in performing a finite element analysis (FEA) is establishing the correct geometry and solid models. The complex geometry of the human anatomy has lead to a surge in computerized anatomical models derived from medical imaging. The techniques and methods discussed in this section will be implemented into the study on developmental hip dysplasia.

1.2.1 Computed Tomography – Based Finite Element Models

Accurately representing human anatomy can be a daunting task for computer-aided design (CAD) software to carry out, and without it, any finite element analysis (FEA) involving the structures composing the human physiology will yield significant uncertainty in results. Technology today, however, has provided an avenue to bypass the need for CAD software in such studies by introducing software that has the capability of translating computed tomography image sets into three-dimensional working models. In generating geometry from CT scans, physicians are not only able to attain highly accurate anatomical models, but also patient-specific geometries. The following studies validate the use of CT image sets in finite element analyses on the hip joint.

In his study, Michaeli et al., evaluated the pressures generated by joint contact for both normal and dysplastic hips [4]. From computed tomography (CT) scans he derived a three-dimensional model of the hip anatomy and applied established hip joint reactions to the appropriate surfaces of the model. The surfaces of interest within the joint were discretized into square elements and the impacting load was divided amongst the individual elements of these surfaces in a manner such that their summation represented the resultant load. The finite element

model calculated the pressures imposed on the hip joint under defined boundary conditions. For verification purposes the pressure was also measured for a cadaveric pelvis and a plastic pelvis model. It was proven that the pressures calculated from the finite element analysis were accurate at designated locations in comparison to the cadaveric hip joint results, and the location of the maximum pressure along with its magnitude agreed with results using a plastic hip [4].

In another study performed by Oonushi et al, the capabilities of the finite element method were used to analyze the deformations of the pelvis as a whole with the pelvic ring and acetabulum being the main focus [15]. In addition, the principal stresses, maximum shear stress, and Von Misses stresses of the pelvis were determined. As before, a three-dimensional computer representation of the hip anatomy was obtained from CT scans to carry out the finite element analysis.

In this study, the mesh distinguished between cancellous bone, cortical bone, subchondral bone, and cartilage. Membrane elements were used for the cortical bone, for it was believed shell elements would introduce error in displacement measurements once muscle loads were applied to the surface. Solid elements composed the inner anatomy while a 1mm layer of membrane elements were attached to the surface to represent the cortical bone as portrayed in Figure 1.8. The solid elements used include tetrahedrons, pentahedrons, and hexahedrons.

Figure 1.8 also demonstrates how the symmetry of pelvis was taken into account in order to decrease computation time and thus simplify the analysis. Upon applying the predescribed mesh to the left side of the pelvis, the boundary conditions were assigned to the line of symmetry to compensate for the right side not being modeled. The femoral head was constrained normal to

the center of the assumed spherical shape of the acetabulum along the weight bearing surface as depicted in Figure 1.9.

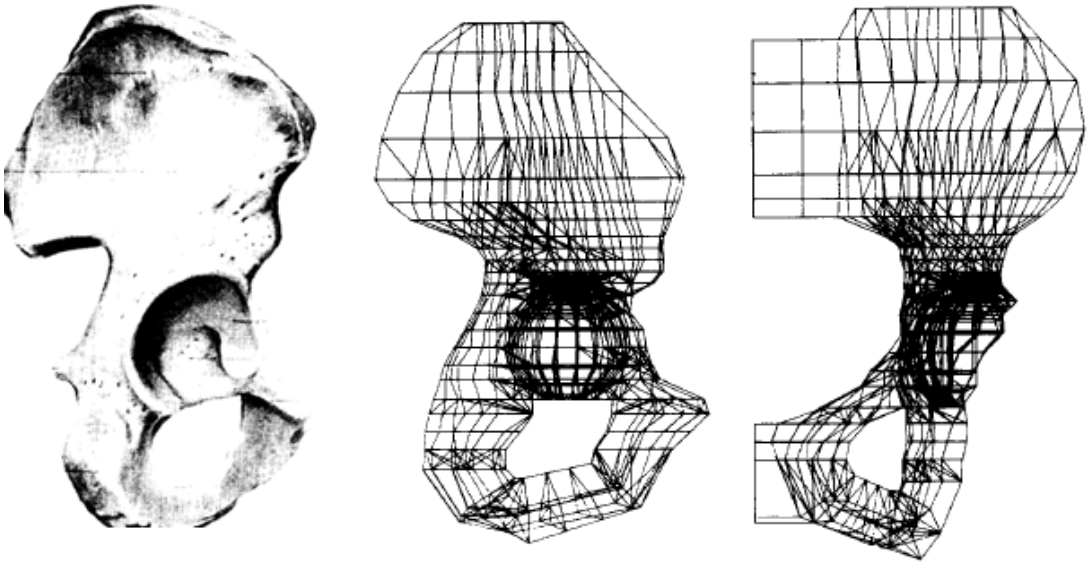

Figure 1.8 Finite Element model of the left side of the pelvis [15]

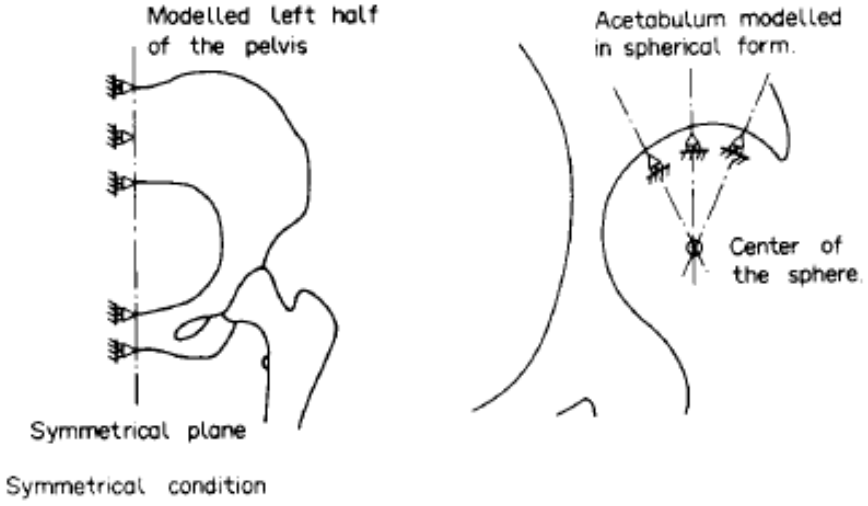

Figure 1.9 Boundary conditions for symmetric, one-sided analysis of the pelvis [15]

The muscles imposed on the model were applied as truss elements limited to axial stiffness and degrees of freedom in the u, v, and w coordinate directions only. The muscles elements attached at two nodal points; their anatomical origin and insertion landmarks [15].

Additionally, the finite element method was used to study dysplastic and healthy hips by Vaverka et al. to compare the depth stress within the two joint conditions (Figure 1.10) [16]. Again, CT image sets rendered computerized models of the hip joint anatomy which were subsequently discretized into elements and nodes as described before. As shown in Figure 1.11, the model included the pelvis, femur, and articular cartilages. The hip abductors were also included and modeled as stiff cables and the analysis was completed in ANSYS 7 software (Figure 1.12) [16].

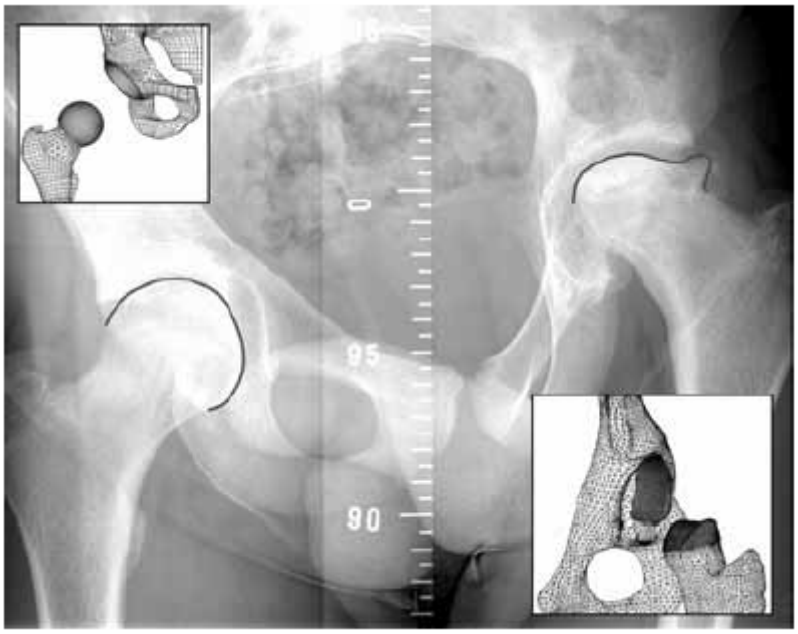

Figure 1.10 Healthy (left) and dysplastic (right) hip joints [16]

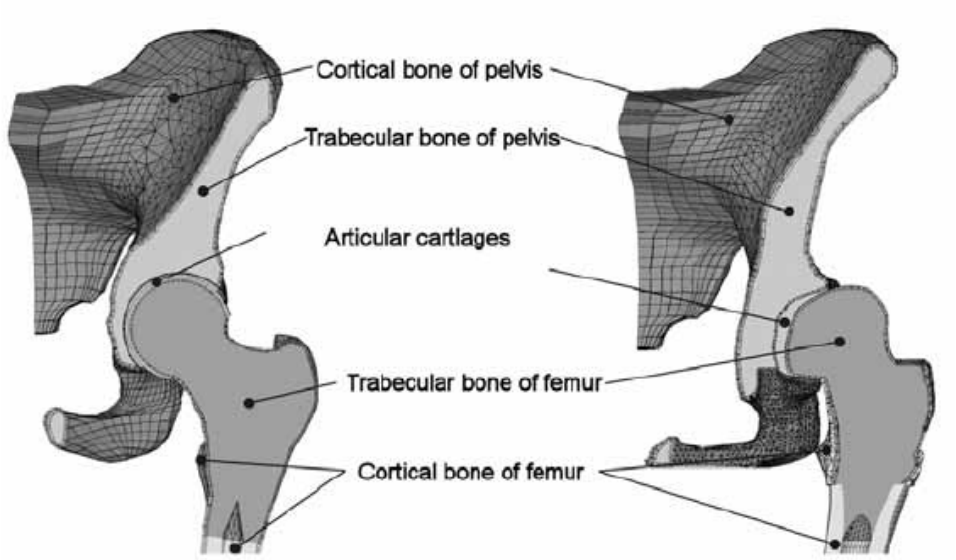

Figure 1.11 Healthy (L) and Dysplastic (R) hip joint finite element models [16]

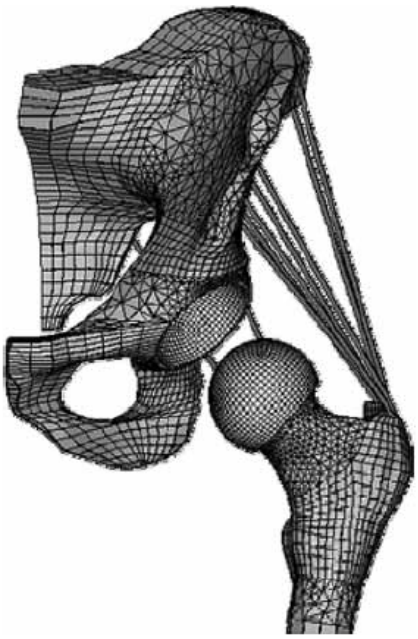

Figure 1.12 Finite element model with muscles represented as stiff cables [16]

1.2.2 Musculoskeletal Models from Magnetic Resonance Imaging

In addition to the bone structure, the other component to a complete finite element analysis on human physiology involves the interacting muscles in the region of interest. In previous studies, muscles had been represented as rods and cables during simulations which may be acceptable for simplified models. However, for more complex muscles such as those that have significantly varying cross sections between their points of origin and insertion or that wrap around other muscles and bony landmarks to reach their insertion points, a simplified model could lead to significant error during simulation. For these more complex muscles, medical image data sets such as magnetic resonance imaging (MRI) can be utilized in the same fashion as the CT scans were to generate bone anatomy in order to develop an accurate muscle model that represents its true volume, interfacing surfaces, and physiological orientation.

In a study focusing on the muscles commonly lengthened to treat children suffering from cerebral palsy, Arnold et al. analyzed the accuracy of muscle-tendon lengths and moment arms of psoas and medial hamstring muscle models derived from MR images from 3 separate cadaveric specimens, and compared results to actual experimental data obtained from the same cadavers [17]. The bony structures and muscles of interest were outlined in each MR image slice and upon connecting adjacent contours with a polygonal mesh, three-dimensional models were composed for each structure (Figure 1.13). Ellipsoidal wrapping surfaces were created within the model to account for underlying muscles not present in the simulation as well as other physiological constraints. Muscle-tendon paths were defined using muscle-specific algorithms for functional ranges of joint motion through normal gait [17].

The findings yielded a maximum error between experimentally determined moment arms and those calculated of 8% for the psoas tendon, 9% for the semimembranosus and 4% for the semitendinosus. The error also remained below 10% of the experimental data for knee flexion moment arms across all muscles modeled. Since the muscle moment arms directly correlate with the muscle-tendon length, these error values are also representative of the accuracy with respect to the experimental length. The study confirmed the use of MRI-based musculoskeletal models can accurately simulate anatomical muscles in kinematic simulations [17].

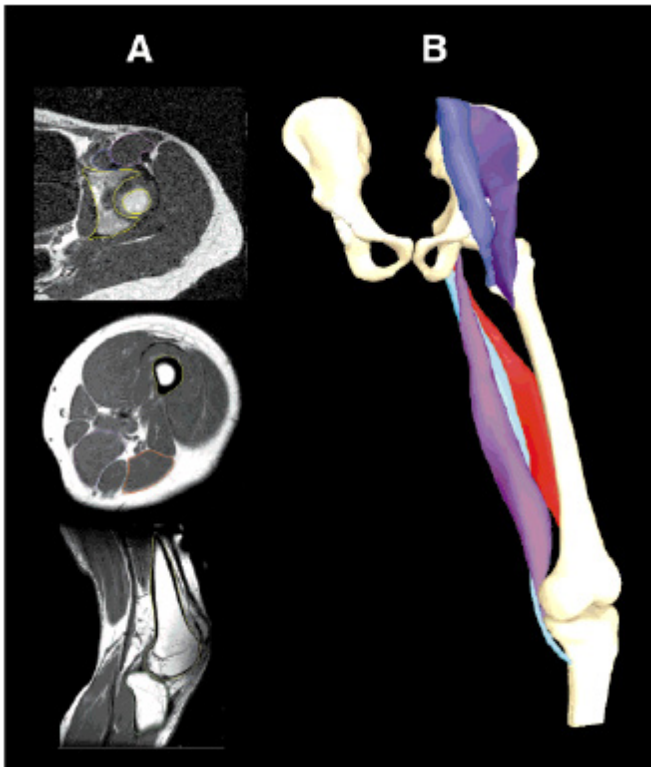

Figure 1.13 3D surface models of bones and muscles derived from MR images [17]

CHAPTER 2
CT-BASED ANATOMICAL MODELING

2.1 Generating an Accurate Three-dimensional Pelvis

An anatomically accurate hip and femur model are essential for performing any computer-based analysis on the hip joint. Without an accurate hip and femur model the correct points of origin and insertion of the interacting adductor muscles would not be feasible. The muscles of interest for this study include the adductor brevis, longus, and magnus along with the gracilis and pectineus muscles. The illiopsoas will also be taken into account when the case of 0^{o} hip flexion is being analyzed. The adductor muscle group acts to reduce the femoral head back into the acetabulum when displacement has occurred; therefore, it is imperative that their points of origin and insertion be precise in order to account for their force vectors properly during simulations.

To achieve three-dimensional representations of an infant pelvis and femur, Orlando Regional Medical Center provided computed tomography (CT) scans of a 14-year-old female and a 6-month-old female each diagnosed with hip dysplasia (Figure 2.1). The CT scans of both patients were individually imported into Mimics (Materialise Inc, Plymouth, MI) software to analyze the images and ultimately produce three-dimensional masks of the anatomies. The CT scans of both patients were sliced transversely in 2 millimeter increments, and captured anatomy ranging from the lower lumbar vertebrae to the region slightly inferior to the lesser trochanter. Since both CT image sets were sliced at 2 millimeters, the 14-year-old patient yielded a more defined three-dimensional masks due to the relative size difference between the two patients; hence the 14-year-old patient was chosen as the model to move forth with for simulation

purposes while the less detailed three-dimensional masks of the 6-month-old was used solely as a scaling reference as described later.

Figure 2.1 CT scans of 6-mo.-old (left) and 14-yr.-old (right) diagnosed with hip dysplasia

In neonates, much of the pelvis along with the femoral head are composed of ossification centers embedded in cartilage. Stemming from an ossification nucleus located within the cartilage, these regions ossify into bone over the first years after birth. The unique material properties of bone and cartilage require a definitive distinction between the two within the models prior to completing a finite element analysis. The Mimics software allowed for the segmentation of the CT scans into color-coded masks representing the bone and various cartilage regions. First, the cartilaginous regions were verified by growing a mask of the 6-month-old hip bone. Using a threshold tool within Mimics, a Hounsfield Unit (HU) range of 500-2000 was specified to contrast the CT images in a manner that highlighted the bone of the hip and blacked out soft tissue. The image contrast made it easy to decipher where bone had not yet ossified

(Figure 2.2). The cartilage will not be displayed at higher HU values due to its lower radiodensity, and thus will appear absent in the three-dimensional mask of the hip bone. The 6-month-old hip rendering will then be used as a reference when masking the cartilaginous regions on the 14-year-old CT images.

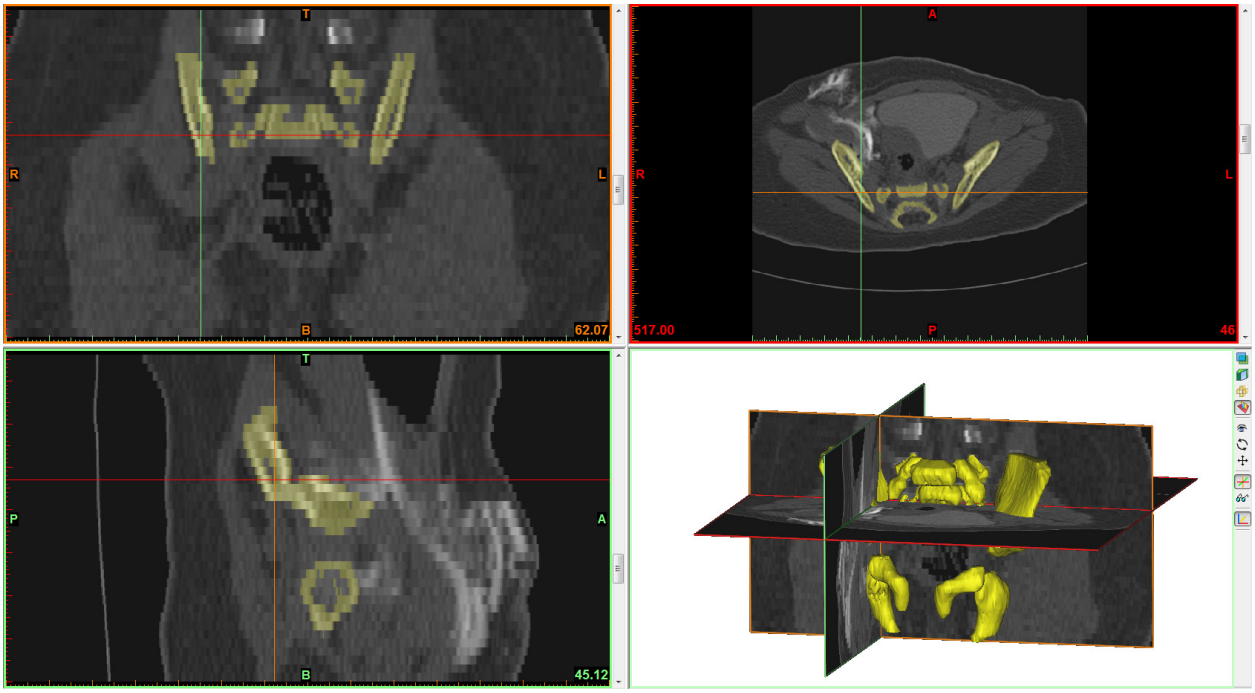

Figure 2.2 Mimics software interface for 6-month-old patient image set; Top (T), Bottom (B), Posterior (P), Anterior (A), Right (R), and Left (L)

Upon calculating a three-dimensional mask of the 6-month-old hip bone using a built-in function of Mimics, the cartilage locations became apparent (Figure 2.3). The 14-year-old images were subsequently segmented in a manner that the cartilage masks agreed with the regions of bone deficiency in the 6-month-old hip rendering. The masks were edited using the

slices composing the CT scans along with the sagittal, coronal, and transverse planes to separate the appropriate regions.

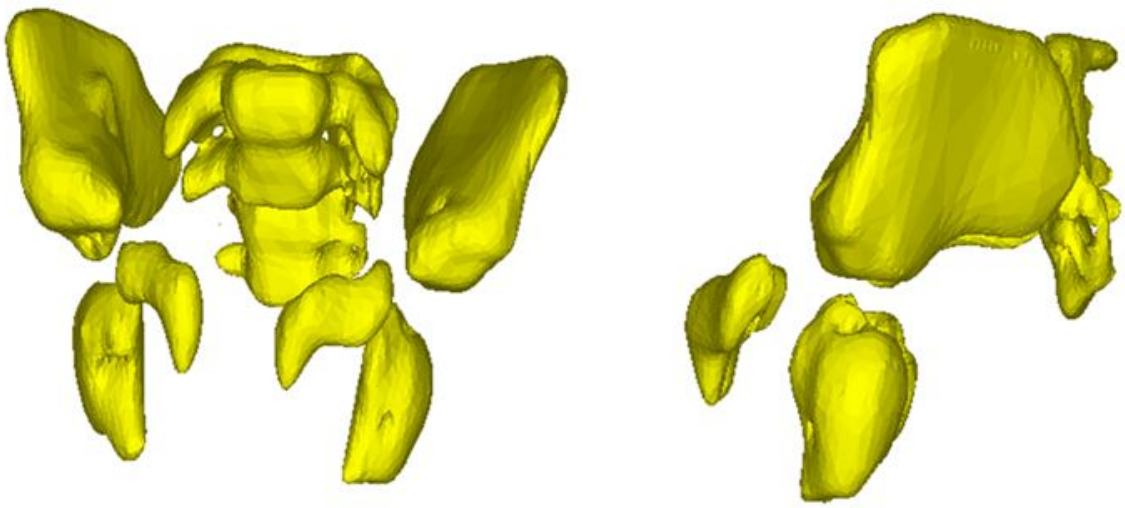

Figure 2.3 Three-dimensional rendering of the bone present in the 6-month-old patient using Mimics software

Once the individual masks for the bone, hip cartilage, and femoral cartilage were grown, three-dimensional representations were calculated within the software producing an anatomically accurate hip and partial femur model that takes into account the cartilaginous characteristics of a neonate hip joint (Figure 2.4). In analyzing Figure 2.5, it becomes apparent that the 14-year-old patient suffered from unilateral hip dysplasia on the left side.

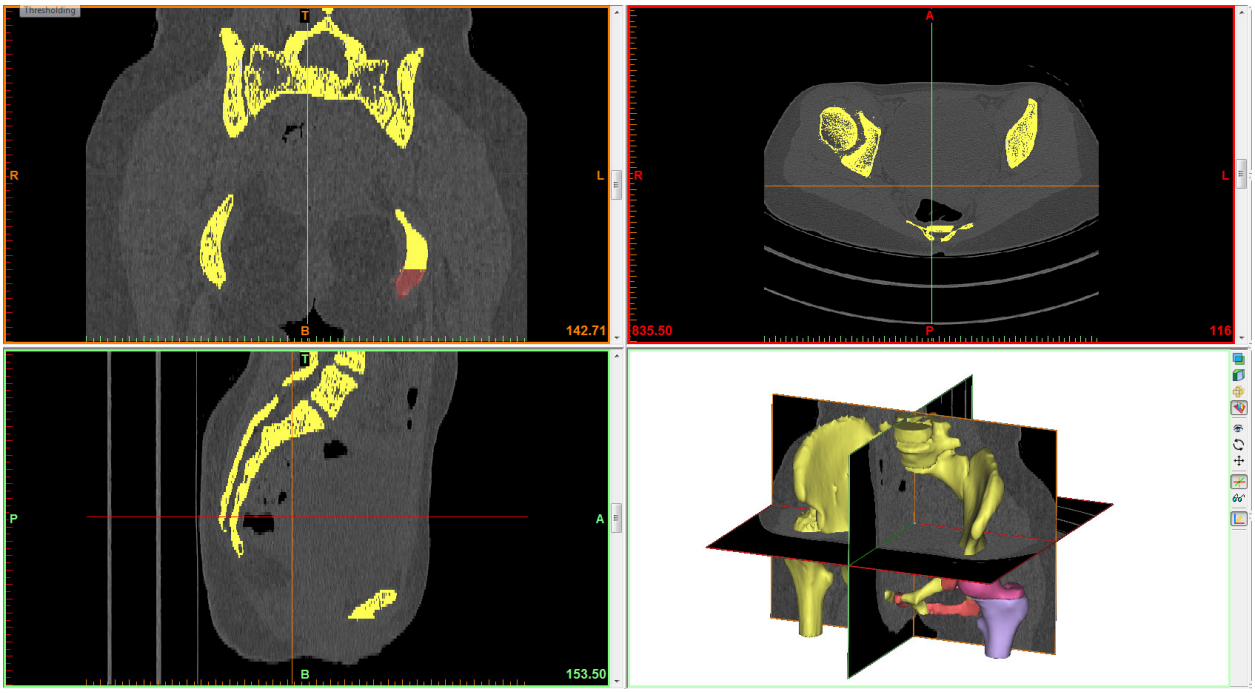

Figure 2.4 Mimics software interface for 14-year-old patient image set

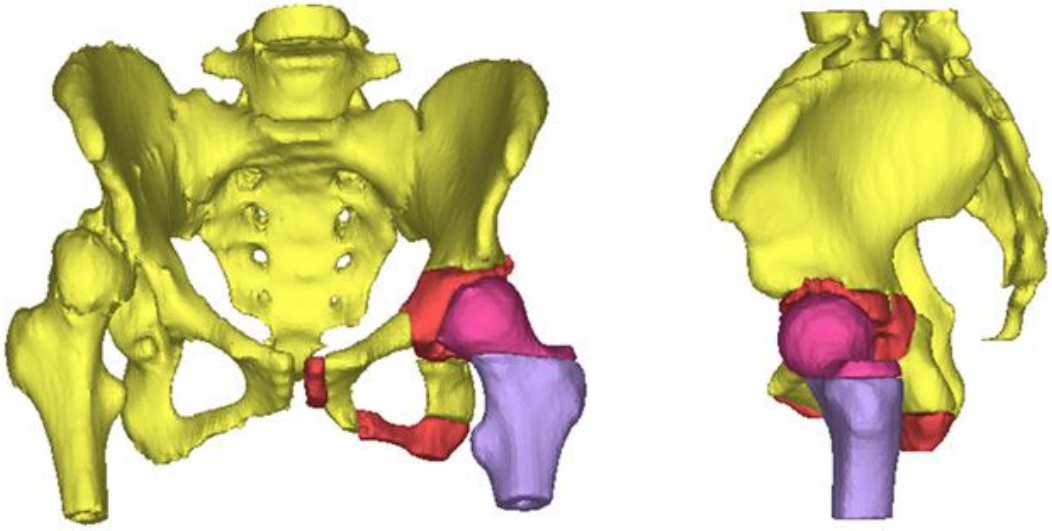

Figure 2.5 Three-dimensional rendering of the 14-year-old anatomy

2.2 Development of a Full Femur Three-dimensional Model

As stated earlier and shown in the displayed models, the femur generated from the CT scan of the 14-year-old patient only extents down from the femoral head to the region just inferior to the lesser trochanter. This partial femur will not suffice for a simulation of the hip joint due to a lack of insertion points for the adductor muscles and an inaccurate mass representation. All of the adductor muscles insert onto the femur further down than what is provided by the 14-year-old model. Due to these deficiencies a CT scan from the Visible Human Project image set that contained a full femur was obtained and imported into Mimics software where a three-dimensional mask was grown in the same manner as the two pelvis image sets (Figure 2.6). The resulting three-dimensional femur model is illustrated in Figure 2.7.

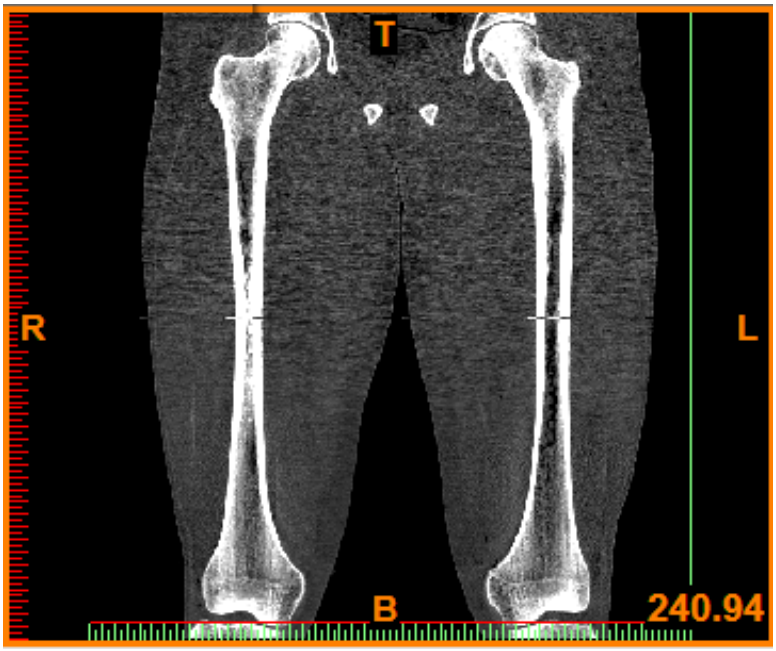

Figure 2.6 CT scan of Visible Human Project image set

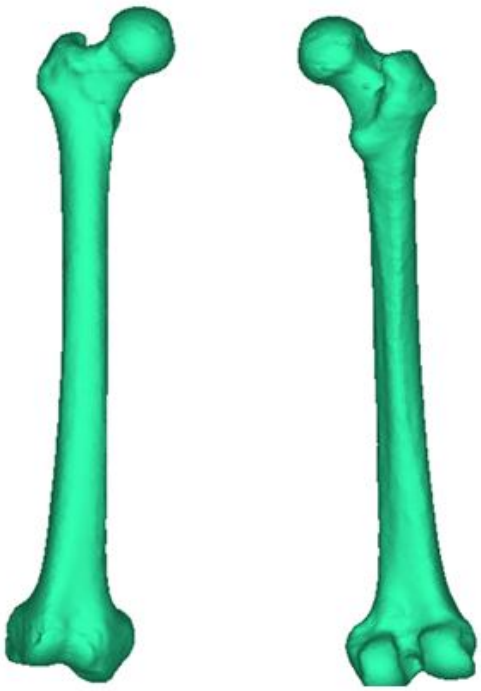

Figure 2.7 Three-dimensional adult full femur computer model

CHAPTER 3
COMPUTER-AIDED PHYSIOLOGICAL ALTERATIONS

3.1 Hip Model Alterations

3.1.1 Scaling the Generated Hip model

Although the hip model of the 6-month-old child was more relevant to the study of neonate hips, the 14-year-old CT scan contained more images, and thus presented a more accurate and defined model. Due to its increased precision and additional geometry, the 14-year-old pelvis regeneration was chosen as the model geometry to base dynamic analysis off of; however, the 6-month-old hip will still be utilized in order to properly scale down the anatomy of the 14-year-old to match that of an infant. The hip renderings of both patients were imported into 3-Matic (Materialise Inc, Plymouth, MI) software to begin the scaling process. The 14-year-old model was first altered to represent a healthy hip joint on both sides. To achieve this, a sagittal midplane was created that split the hip into two even halves which was then used to divide the hip. Subsequently the diseased right side was removed and the healthy left side was mirrored about the midplane leading to two congruent halves both of which represented a healthy hip joint (Figure 3.1). The deformed right acetabulum remaining as a result of the displaced femoral head of the 14-year-old patient was not desired for simulation purposes. Figure 3.2 displays the unscaled 3-Matic models of the 6-month old and 14-year-old patients side by side.

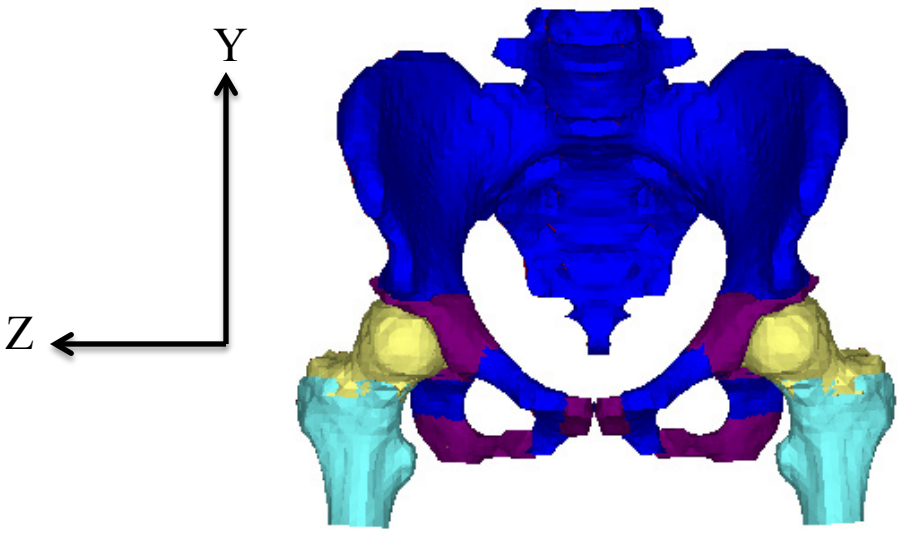

Figure 3.1 Unscaled 3-Matic model of 14-year-old patient with healthy hips

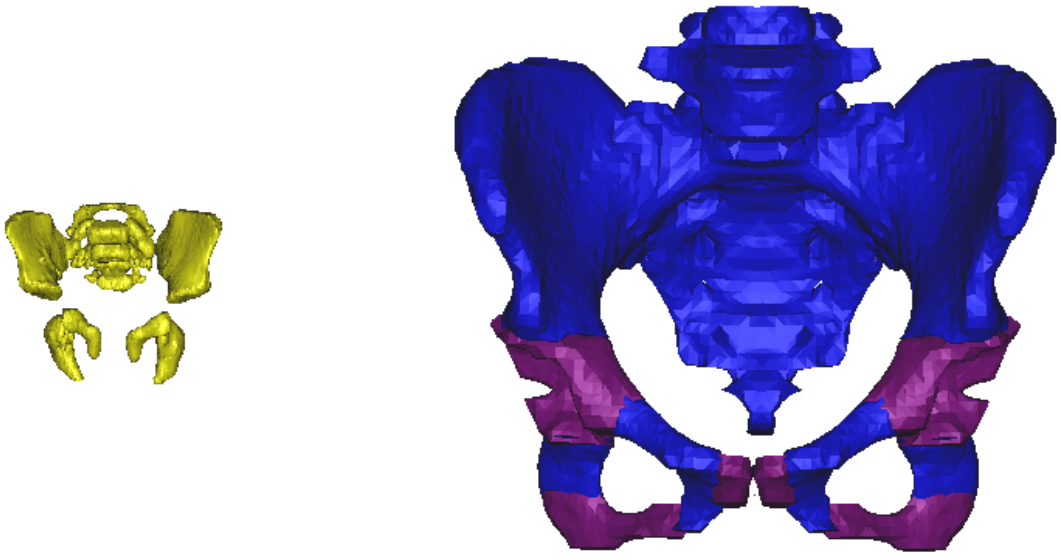

Figure 3.2 Side-by-side comparison of the 6-mo.-old model (left) to the 14-yr.-old model (right)

Initially, identical measurements were taken on the ilium of the infant hip model and the teenage model in order to calculate scaling factors in the x, y, and z-directions. Due to the ambiguity of the infant hip model, the scaling factors proved inaccurate in magnitude, however, the nonuniform values did justify the assumption that the hip bone does not grow isentropically. With the hip models superimposed on top of one another, these scaling factors were adjusted until the two models overlapped. In aligning the models, the acetabula were paid particular attention to as well as the anterior superior and inferior iliac spines since these were more profound on the infant model. Since the 6-month-old hip lacked a developed acetabula the models were aligned in a manner that the overlapping acetabula of the 14-year-old filled the vacancy on either side. The ultimate resulting scaling factors for the x, y, and z-directions were 0.35, 0.30, and 0.35 respectively. It should be noted that although the hip is being used to determine the scaling, the partial femur is being scaled by the same factors. The superimposed scaled 14-year-old hip model and infant model can be observed in Figure 3.3.

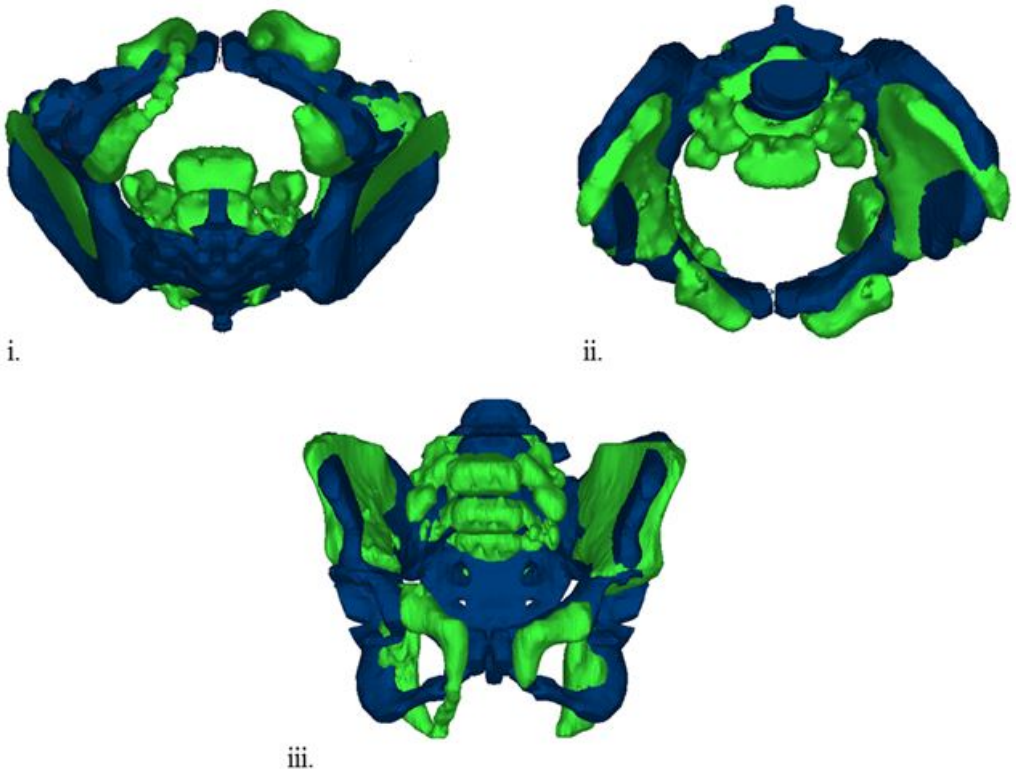

Figure 3.3 Superposition of scaled 14-year-old and 6-month-old pelvis. (i) Inferior view, (ii) Superior view, (iii) Front view

3.1.2 Modifying the Pubis and Ischium

Upon examination of the scaled 14-year-old model and 6-month-old model, it was noted that the 6-month-old hip appears to have a slightly shallower iliac fossa in comparison to the 14-year-old patient and the angle of the ischia do not agree resulting in a wider pelvic outlet diameter for the scaled hip model. The differences in the iliac fossa were deemed negligible;

however, the ischium and pubis regions deviated significantly and will need to be modified to match that of infant.

The adductor brevis, adductor magnus, adductor longus, pectineus and gracilis muscles all originate from either the ischium or pubis regions of the hip bone. It is therefore imperative that the misalignment recognized between these two regions of the scaled and infant hip be corrected. The discrepancy was attributed to the natural widening of the pelvic inlet that teenage females endure during puberty; a stage which would not yet influence an infant hip. Features within 3-Matic will be used to perform the correction.

Initially, two datum planes were created in order to separate the ischium and pubis from the rest of the hip in order to modify that localized region without affecting the remaining model geometry (Figure 3.4). Figure 3.5 displays the model upon completion of this division.

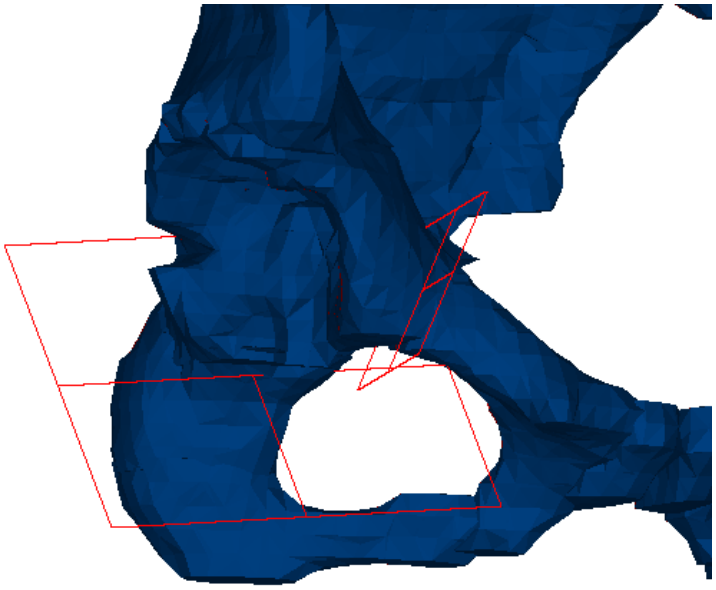

Figure 3.4 Planes defined to segment the pubis and ischium

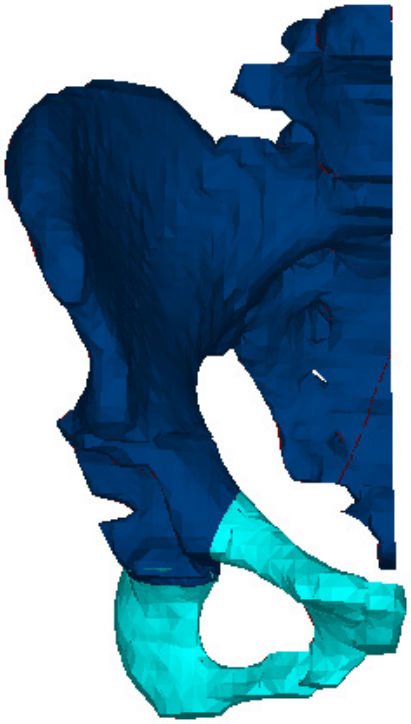

Figure 3.5 Final segmented pubis and ischium of 14-year-old model

Next, this separated region was rotated in order to align with the infant ischium and pubis. The ischial ramus on the left side of the infant hip was manually added into the model in order to help with the alignment of the scaled ischium. Figure 3.6 shows a superior and inferior view of the adjusted alignment of the scaled ischium and pubis. A superposition and side by side comparison of the final scaled hip model with the infant hip can be seen in Figure 3.7 and Figure 3.8 respectively.

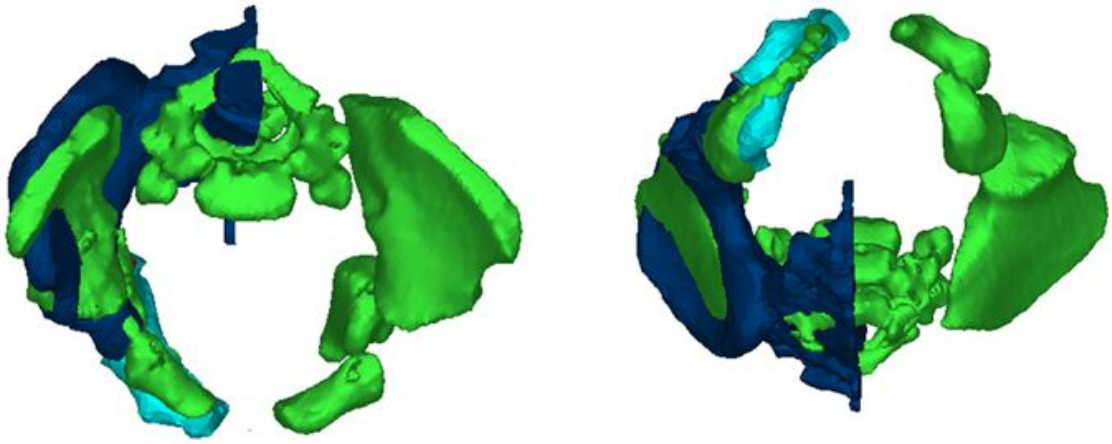

Figure 3.6 Superior (left) and inferior (right) view of the adjusted ischium and pubis

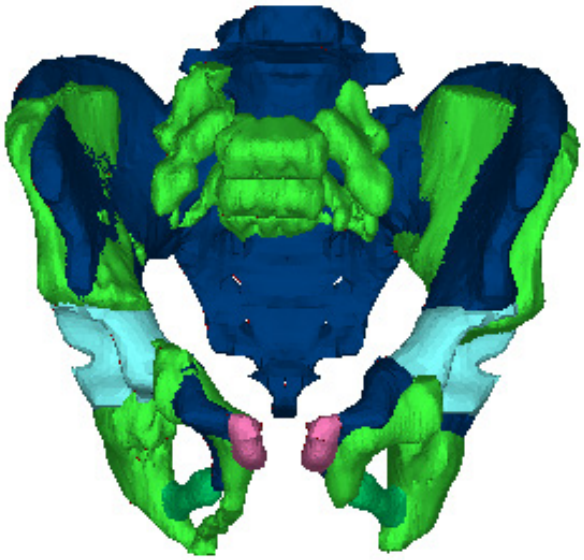

Figure 3.7 3-Matic superposition of the 6-month-old model and scaled 14-year-old model

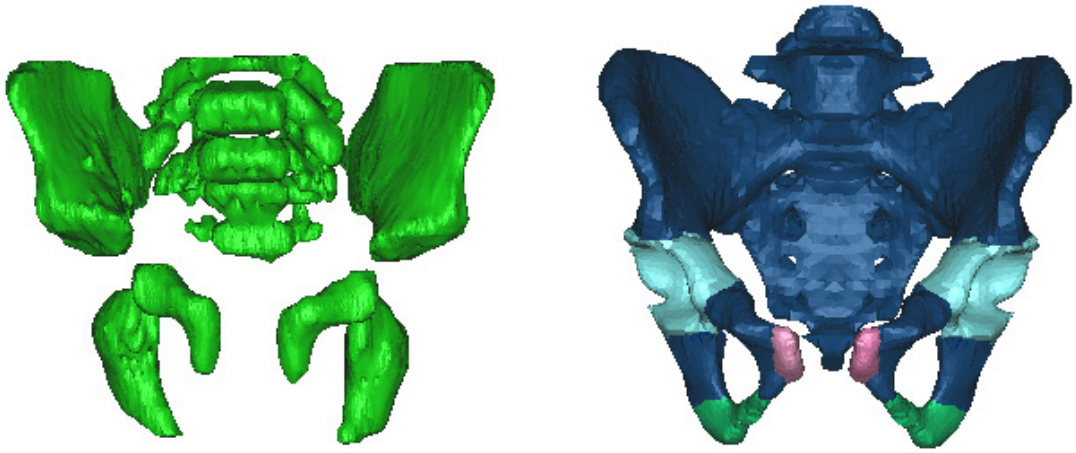

Figure 3.8 Side-by-side comparison of scaled 14-year-old pelvis with 6-month-old pelvis

3.2 Femur Model Alterations

3.2.1 Scaling of the Full Femur Model

Since the Visible Human image set is of a 38-year-old, the resulting three-dimensional femur mask must be scaled down as the 14-year-old hip and partial femur models were, but using a new set of scaling factors. This time, the already scaled partial femur of the 14-year-old will be used as the scaling reference to scale down the adult full femur model.

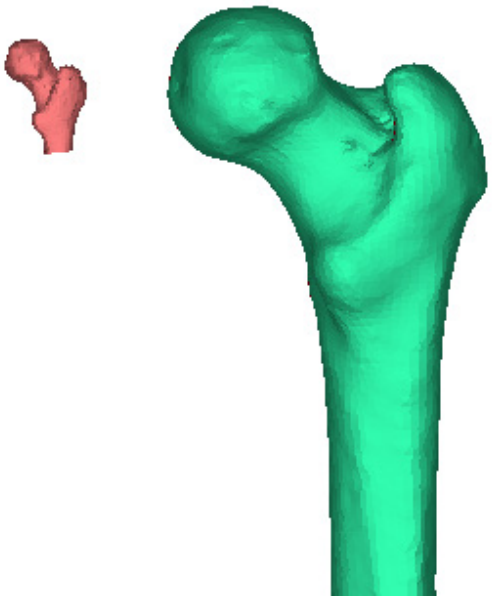

Figure 3.9 Comparison of scaled 14-year-old partial femur and the Visible Human model

The scaling factors for the x and z-directions of the adult femur were measured by superimposing the model over the already scaled partial femur of the 14-year-old patient; however, due to the lack of inferior anatomical geometry in the 14-year-old femur model as shown in Figure 3.9, it was determined not to be sufficient enough to deduce a scaling factor for the y-direction. To obtain a more accurate scaling factor for this direction, the tables listed by Robert Hensinger depicting bone growth of both the pelvis and femur from birth to 18 months were referenced in order to determine the appropriate femur length that corresponded with the measured pelvic height of the 6-month-old and scaled 14-year-old models [6]. The pelvis height measurement was taken along the diagonal that began at the tip of the ilium to the base of the ischium bone as demonstrated in Figure 3.10. The femoral length was measured between the two epiphyseal plates; the first located at the superior surface of the lesser trochanter and the

inferior surface of the greater trochanter and the second located just above the femoral epicondyles as shown in Figure 3.11.

Interpolation of the table listings revealed that the pelvic height of the generated infant hip models actually correlated with the 50th percentile of a 2.2-month-old (10-week-old) full term female infant despite the patient being 6 months of age. Table 3.1 displays the pelvic height for a 50th percentile 6-month-old according to Hensinger and the percent the 6-month-old patient models vary from this mean value [6]. It should be noted that the Pavlik harness is used as a means of treatment for infants between the ages of 0-6 months; therefore, although the 6-month-old patient has a lower percentile pelvis size, the models generated are still applicable to the study since a 10-week-old would be a valid patient for the treatment.

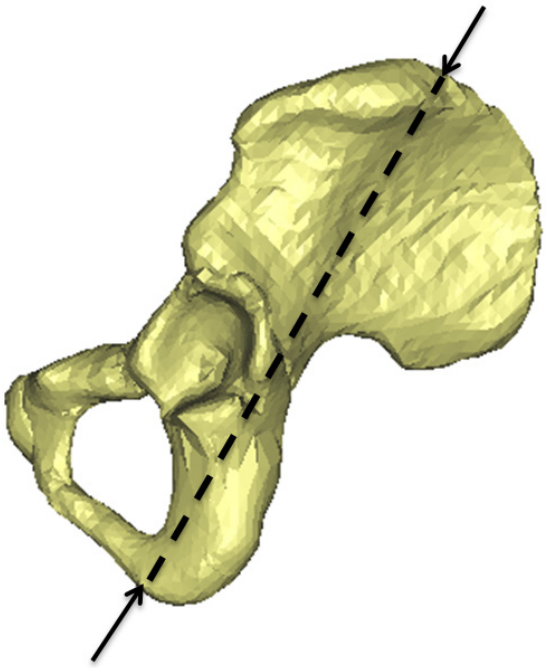

Figure 3.10 Pelvis height measurement

Table 3.1 Summary of Pelvic Height Measurements [6]

Source	Hensinger 6-mo-old	6-mo-old model	14-yr-old scaled model
Pelvic Height (mm)	80.5	67	68
% Variance	-	16.70%	15.50%

Figure 3.11 Femoral length measurement

In order to ensure the femur agreed with the pelvis proportionally, the femoral length of a 10-week-old was hence deduced from growth charts. After interpolation of the tables, the 50th percentile femoral length of a female 10 weeks of age resulted in 8.85cm. To generate a femur

model that agreed with this length, a scaling factor of 0.249 was applied to the Visible Human full femur in the y-direction.

In order to determine scaling factors for the x and z-directions, the adult femur model was superimposed over the already scaled partial femur model as shown in Figure 3.12, and the factors were varied until the geometries matched. In superimposing the two anatomies, aligning the femoral heads with respect to size and location was the primary means of verifying the x and z scaling factors. The femoral head was chosen as the primary reference surface since it articulates with the acetabulum, and is thus an influential component in the hip joint. Also, it is important to sustain a concentric femoral head and acetabulum to represent a healthy configuration during analyses; therefore because the femoral head of the partial femur was scaled by the same parameters as the pelvis model it already lies concentrically with respect to the acetabulum. Scaling the adult femoral head to match this surface ensures the preservation of this relationship in the complete femur model.

As with the scaling of the 14-year-old pelvis and partial femurs, the scaling factors for the adult femur model were nonuniform with respect to the x, y, and z-directions. The global coordinate system agrees with the studies on hip biomechanics carried out by Dostal and Andrews [18]. After several iterations the scaling factors were determined to be 0.23, 0.249, and 0.22 for the x, y, and z-directions respectively.

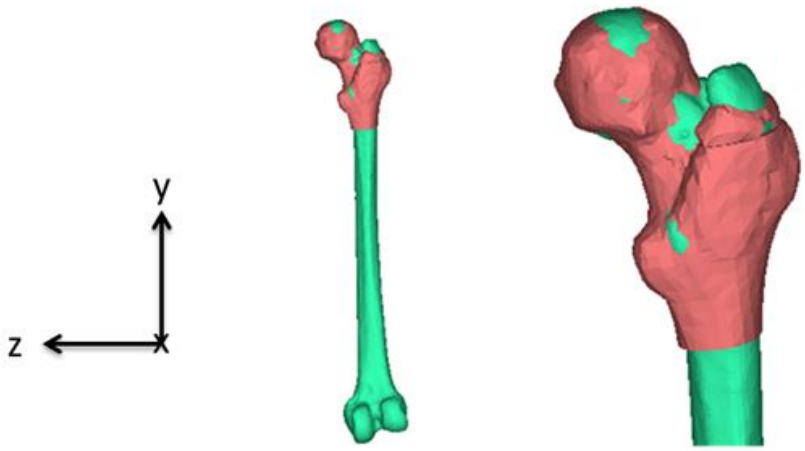

Figure 3.12 Superposition of scaled adult femur with the already scaled 14-year-old femur

The resultant femoral head diameter of the scaled full femur model was measured to be 12.2 mm. According to Hensinger, this diameter falls just below the average for femoral head diameter of a 10-week-old as displayed in Figure 3.13 [6]. Despite being a few millimeters below the average, the diameter measurement still follows the natural trend of the plot. Aligning correctly with the acetabulum of the scaled pelvis holds more importance than agreeing with the mean diameter, for anatomies are unique in all dimensions in comparison to mean measurements, but the size of the femoral head and acetabulum must coexist in order for the joint to articulate correctly. Furthermore, the acetabular shape of the scaled pelvis comes in close agreement with the mean ratio calculated for a child 10 weeks of age with a value of 39.1%. The percentage represents the ratio of the acetabular depth to the diameter [6]. The percentage increases after birth and levels out once development has ceased and the acetabulum exhibits a hemispherical shape.

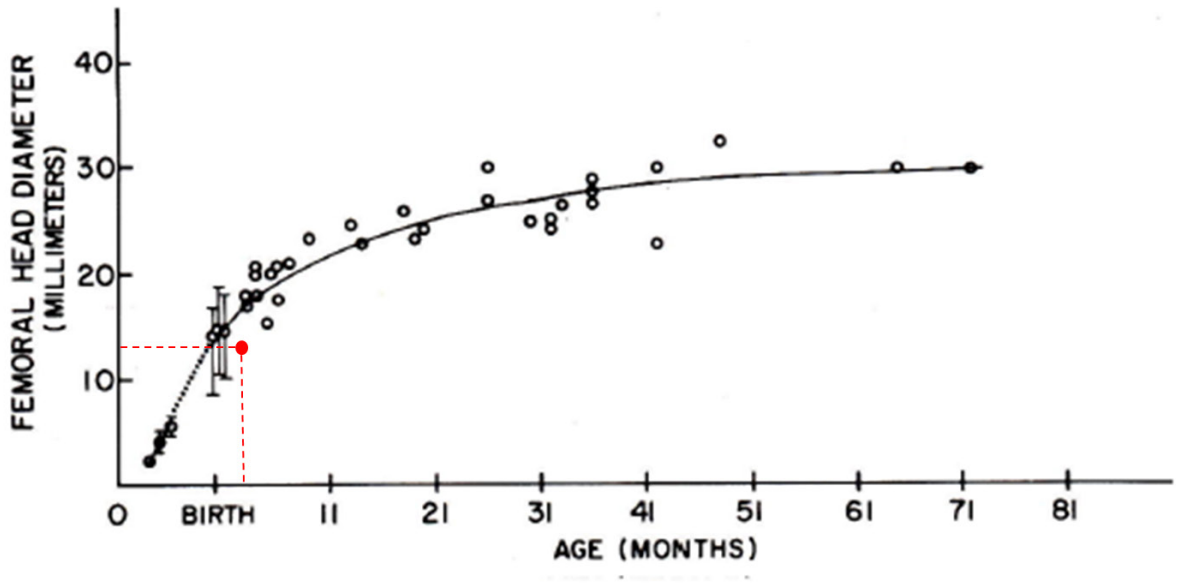

Figure 3.13 Femoral head diameter as a function of age, modified from [6]

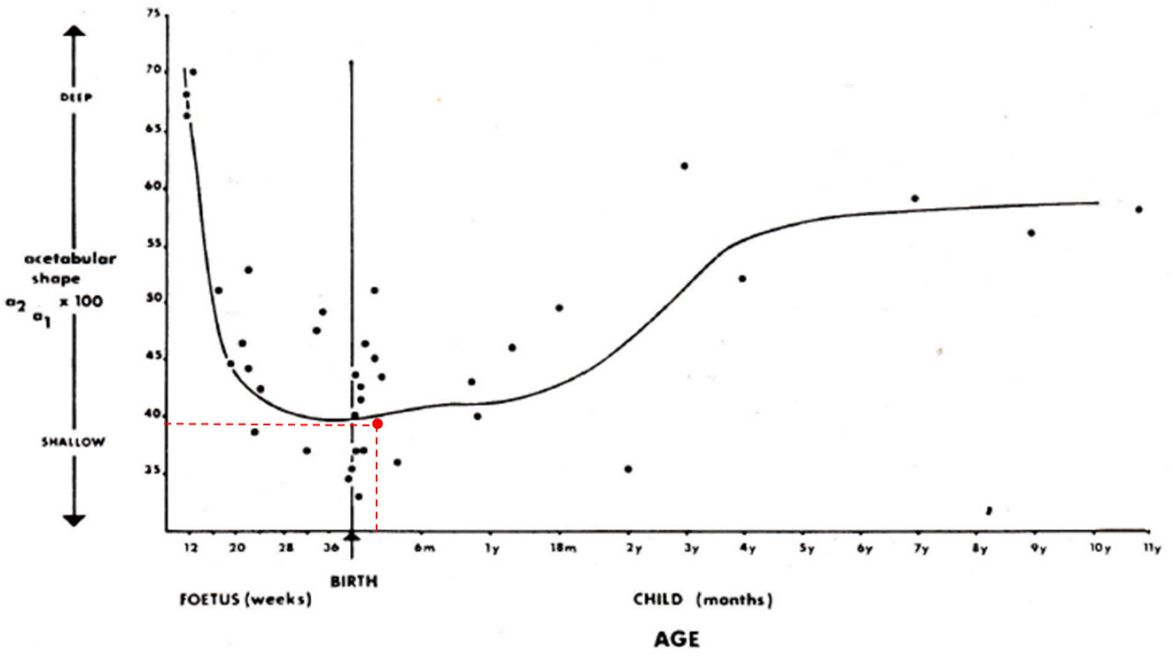

Figure 3.14 Acetabular shape as a function of age, modified from [6]

3.2.2 Segmentation of the Scaled Femur

A typical femur consists of cancellous bone enclosed in a thin outer layer of cortical bone with the exception of the hollow portion of the diaphysis where the marrow cavity exists. As with most long bones in the human skeletal system, the femur starts as cartilage and begins to ossify and lengthen during embryotic development; however, at birth some of this cartilage is still prevalent in the composition of the femora. In newborns, much of the femoral head and neck region has yet to ossify and still remains as cartilage as shown in the radiograph in Figure 3.15[19]. Additionally, the distal region near the epicondyles has also not yet ossified in neonates (Figure 3.16) [20]. These unique characteristics exhibited by infants must be appropriately accounted for in order to attain an accurate finite element model. This nonhomogeneous nature of the infant femur was addressed by segmenting the three-dimensional scaled femur model in 3-Matic to correspond and accurately depict the regions of cartilage and cortical bone. Since the two regions where cancellous bone propagates at the proximal and distal ends of the femora have yet to ossify, cancellous bone will be neglected in the segmented infant femur model.

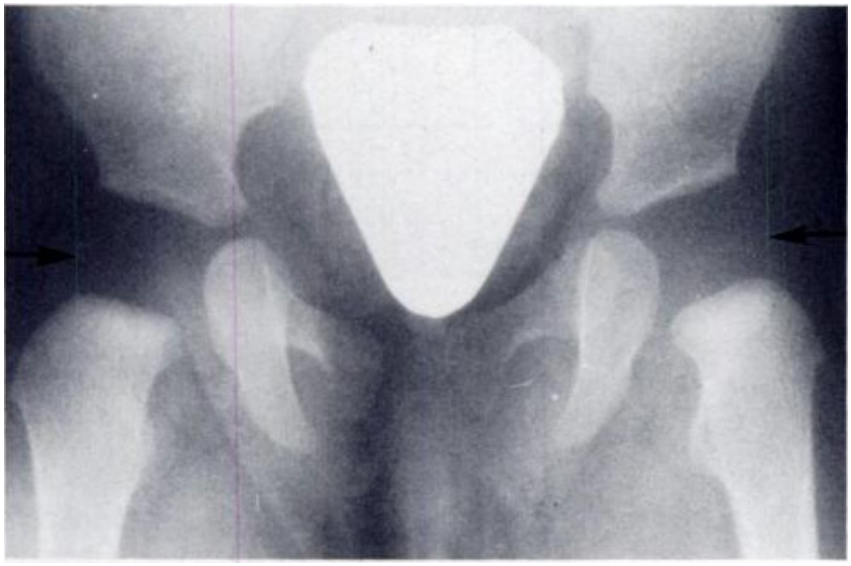

Figure 3.15 Pelvic radiograph of 6-month-old girl [19]

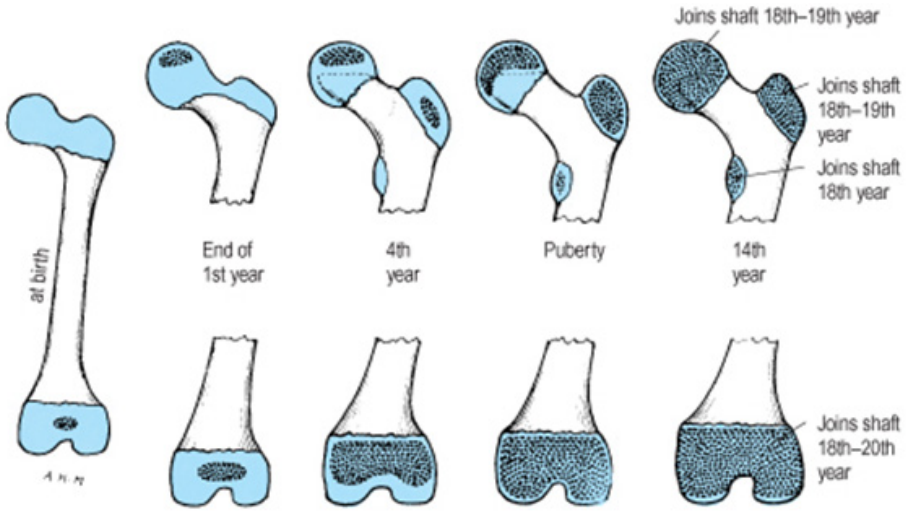

Figure 3.16 Femur postnatal development [20]

To establish the inner surface where the cortical bone terminates and the medullary cavity exists, the CAD toolset within 3-Matic was utilized to offset the outer cortical bone surface a distance of 1.87mm inward. This offset distance was determined by measuring the thickness of

the cortical bone at various points along the femoral shaft of the Visible Human patient beginning below the lesser trochanter and moving distally down the shaft. Table 3.2 shows that for each thickness measurement, the ratio to the overall diameter of the shaft at the corresponding location was calculated.

Table 3.2 Cortical bone thickness measurements of Visible Human femur

VISIBLE HUMAN PATIENT MEASUREMENTS					
Cortical Thickness (mm)	7.11	8.21	8.35	7.1	5.85
Overall Diameter (mm)	31.35	30.49	28.39	28.92	32.99
Cortical Ratio	0.227	0.269	0.294	0.246	0.177
AVG. RATIO	**0.243**				

These measurements were made using the density contrast provided by the CT images of the Visible Human patient in the transverse plane as demonstrated in Figure 3.17. The ratios along the shaft were then averaged and applied to the average diameter of the scaled femoral shaft to yield the offset distance representative of the cortical bone thickness for a 10-week-old infant.

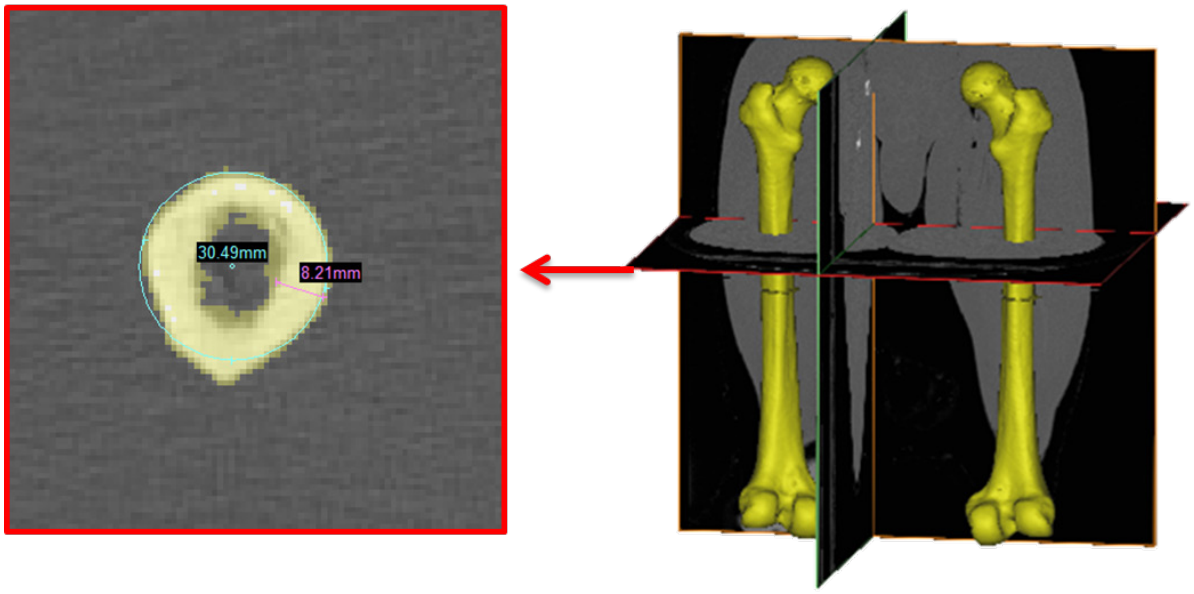

Figure 3.17 Cortical bone thickness measurements using CT data

The segmentation of the two cartilage regions were near the proximal and distal epiphyseal plates respectively. A simplified femur model with segmented regions distinguishing cartilage and cortical bone can be seen in Figure 3.18. A final scaled model of the infant pelvis including full femurs is displayed below in Figure 3.19.

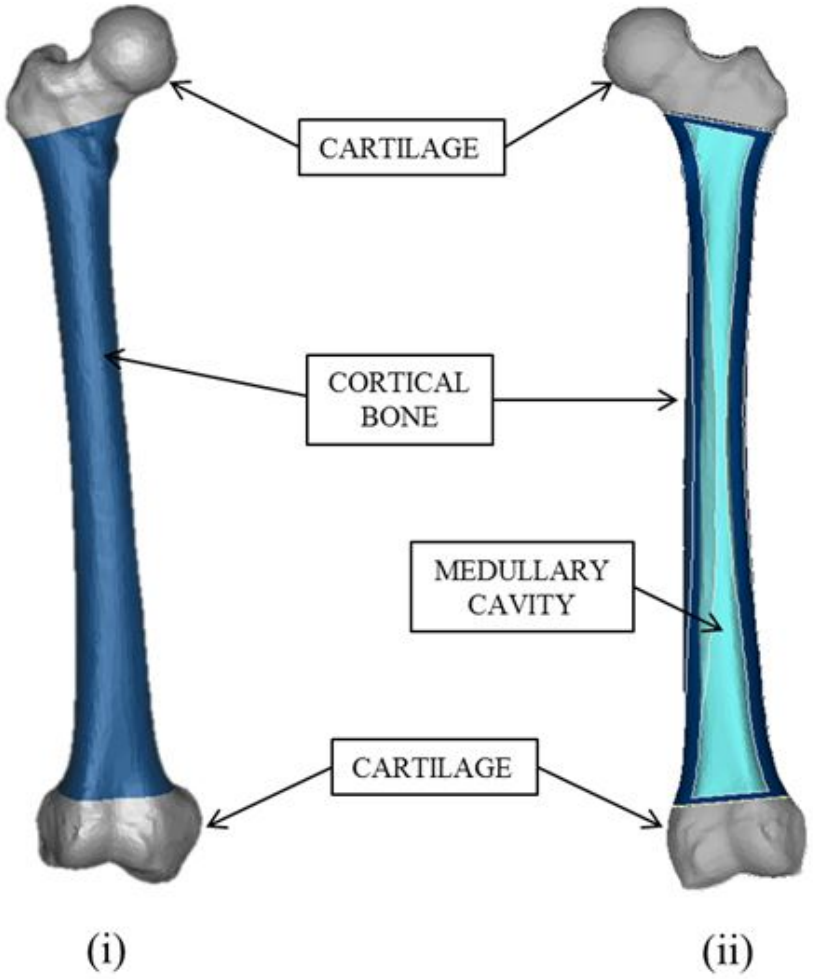

Figure 3.18 Three-dimensional infant femur model (i) complete view and (ii) cross-sectional view with distinguished cartilage regions

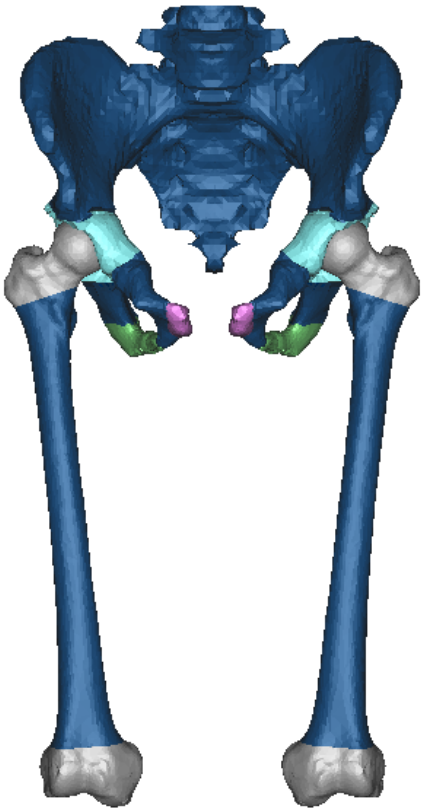

Figure 3.19 Final scaled 3-Matic pelvis and femur models representing a 10-week-old infant

CHAPTER 4
MECHANICAL PROPERTIES

4.1 Background

In the pelvis and femur exists regions of cortical and cancellous bone along with cartilage, all of which exhibit unique mechanical properties that individually contribute to the behavior of a functioning hip joint. Furthermore, these material regions differ in a neonate anatomy in both location and expanse when compared to an anatomically developed hip joint. Due to the natural propagation process of cancellous bone throughout cartilaginous regions in a newborn pelvis and femur, cartilage is much more prevalent in a neonate model as discussed in previous chapters. Defining mechanical properties for these distinguished regions is essential in order to perform a finite element or dynamic analysis.

Cortical and cancellous bones make up the two types of ossesous tissue in the body. Cortical bone serves as the hard outer shell to many bones in the skeletal system and is much denser than cancellous bone. In addition to being less dense, the cancellous bone also exhibits softer and less stiff characteristics in comparison to the cortical bone that encases it. The low density of the cancellous bone can be attributed to its matrix structure which allows blood supply to route through the bone, metabolic activity, and energy absorption from joint contacts. On the other hand, cartilage covers joint interfaces to mitigate friction during mobility and typically does not contribute to structural stability in the hip joint; however, in the infant anatomy this cartilage not only composes the interfacing surfaces of the hip joint but the surrounding structures as well.

4.2 Literature Review

Numerous studies in literature performed on the hip joint note the mechanical properties of the pelvis and femur. Table 4.1 below lists the bone properties recorded in these studies for the two articulating structures. The average modulus of elasticity for femoral cancellous bone was found to be 378 MPa with a standard deviation of 29.103 MPa. The average modulus of elasticity for femoral cortical bone resulted in 17.66 GPa with a standard deviation of 1.013 GPa. As for the pelvis region, Spears et al. documented the use of 100 MPa and 5600 MPa for cancellous and cortical bone respectively in a finite element model analysis on hip replacements [25].

Table 4.1 Cortical and cancellous material properties in the hip joint

Source	Bone Region	Location	Direction of Analysis	Modulus of Elasticity (MPa)	Poisson Ratio
Brown [21]	Cancellous	Femur	Both	345	0.3
Ross [22]	Cancellous	Femur	Long.	389	-
Taddei [23]	Cancellous	Femur	Both	590	-
Taylor [24]	Cancellous	Femur	Both	400	0.33
Spears [25]	Cancellous	Hip	Both	100	0.3
Ross [22]	Cortical	Femur	Long.	17000	0.3-0.6
Ross [22]	Cortical	Femur	Trans.	11500	-
Polgár [26]	Cortical	Femur	Both	17000	0.33
Rohlman [27]	Cortical	Femur	Both	18000	-
Taddei [23]	Cortical	Femur	Both	19300	-
Taylor [24]	Cortical	Femur	Both	17000	0.33
Spears [25]	Cortical	Hip	Both	5600	0.3

Although the cancellous properties of the femur will not be implemented in the study of an infant, it was still included in this data collection in order to provide a comparison to the cancellous bone properties of the hip. As portrayed in the data, the elastic moduli for both bone tissues in the hip decreases in comparison to the femur. However, the poisson ratios for both bone tissues regardless of its location in the hip joint are very similar in value.

Athanasiou et al. performed a study investigating the mechanical properties of the articular cartilage covering the acetabulum and femoral head which were divided up into 6 and 8 distinct regions respectively [28]. The values for these regions were averaged to yield an average elastic modulus of 1.186MPa and average poisson ratio of 0.039 for the femoral articular cartilage and an average modulus of 1.236MPa and average poisson ratio of 0.0435 for the acetabular articulate cartilage [28]. The largest value in the entire hip joint belonged to the superomedial region of the femoral head which had an aggregate modulus of 1.816 MPa which is 41% greater than the modulus of its articulating surface on the acetabulum [28].

4.3 Discussion

Whether or not these bone and cartilage properties agree with the corresponding regions present in early anatomical development is still to be determined. The data collected from the literature review pertained to adult anatomies; therefore a correlation to early childhood must be established. The varying material composition of the infant hip joint from the adult could have a significant effect on the biomechanics of the joint and the mechanism for hip reduction.

The articular cartilage properties recorded by Athanasiou et al. were for the surface regions that interface the hip joint and thus involved thicknesses less than 2 mm; however, for

the infant hip model the cartilage penetrates much further than just the articulating surfaces and serves as a structure in addition to a contact surface [28]. Instead of just a thin layer of articular cartilage, the neonate exhibits the predecessor form where the entire femoral head and neck region and acetabular cup are completely cartilage. This increase in cartilage thickness could significantly alter the previously measured articular cartilage mechanical properties.

Additionally, the difference in age and hence anatomical development could lead to divergence between the mechanical properties as well. Armstrong et al. proved that the equilibrium modulus of articular cartilage only marginally decreases with age as shown in Figure 4.1, but this decrease could still be substantial when analyzing a neonate [29]. These findings were based on the water content in cartilage as age increases.

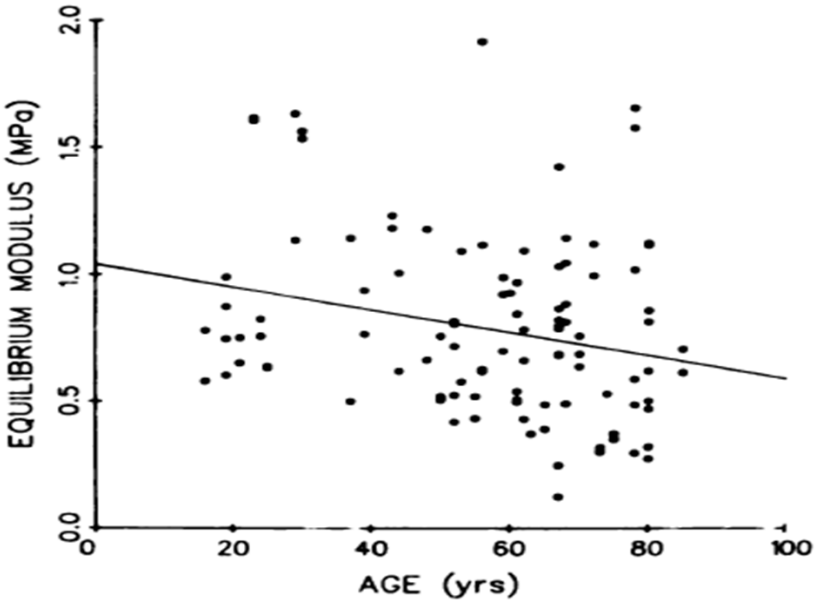

Figure 4.1 How equilibrium modulus of articular cartilage changes with age [29]

The same age correlation needs to be developed for the cortical and cancellous bone properties as well. Due to a lack of literature on the bone mechanical properties in infants, it will be difficult to generate an accurate relationship without experimental data. Nonetheless, Wirtz et al. derived a relation between the elastic modulus and bone density for both femoral cancellous and cortical bone [30]. Equation (1) and (2) displays equations for the elastic modulus in the axial and transverse directions for cortical bone while Equation (3) and (4) represents the equations derived for cancellous bone tissue of the femur. The equations were deduced from a collection of literature studies involving fresh cadaveric femurs.

Femoral Cortical Bone:

$$E_{axial} = 2065\rho^{3.09} \quad (1)$$

$$E_{transverse} = 2314\rho^{1.57} \quad (2)$$

Femoral Cancellous Bone:

$$E_{axial} = 1904\rho^{1.64} \quad (3)$$

$$E_{transverse} = 1157\rho^{1.78} \quad (4)$$

Furthermore, a study performed on fresh autopsy femurs of infants, recorded average values for the ultimate tensile stress, ultimate tensile strain, and tangent modulus of elasticity in tension for the cortical bone to be 10 N/mm2, 1.850%, and 1012.9 kg/mm2 respectively [31]. The quantified modulus value can be applied to the equations derived by Wirtz et al. to measure accuracy, and hence validate or invalidate the usage of the equations for infant properties. The relations could be explored or derived for hip properties as well.

Peng et al., establishes a method to attaining these densities using CT scan data in a study comparing the isotropic and orthrotropic material assignments for double-leg standing and single-leg standing loading conditions [32]. Using the Hounsfield unit (HU) values from CT scans, a linear relation was derived to calculate the density by finding the maximum HU value and correlating it to the cortical bone density and then using the density of water which has a standardized HU of 0. This linear relationship is displayed in Equation (5) where ρ_α represents the apparent bone density in g/cm^3 [32]. These CT-derived densities could be inserted into the power law equations for elastic modulus.

$$\rho_\alpha = 1 + 7.185 \times 10^{-4} \, HU \qquad (5)$$

Each of these materials were treated as regionally homogeneous, isotropic and linearly elastic in literature, and will hence be treated in this manner in the infant finite element model. Once these material regions are properly assigned mechanical properties, the finite element model will be prepared to accept boundary and load conditions and subsequently perform a complete analysis.

CHAPTER 5
ORIENTATION OF THE ILIOPSOAS TENDON

5.1 Background

The iliopsoas tendon serves as the means of attachment for the iliopsoas muscle, composed of the psoas major and iliacus muscles, to the lesser trochanter of the femur. As a whole, the iliopsoas muscle acts as a strong flexor of the hip while the psoas major muscle has the ability to flex the torso laterally. The muscle exhibits an hour-glass shape and wraps anteriorly over the hip joint before inserting onto the lesser trochanter. In practice, the iliopsoas tendon has been deemed an obstruction for hip reduction in infants suffering from developmental hip displacement. Physicians commonly release the tendon surgically in order to expose the hip joint during open reduction procedures as well as to avoid re-dislocation during patient recovery. Since reduction methods such as the Pavlik harness require the femur to be abducted and flexed, the question arises as to whether or not the iliopsoas tendon remains an obstruction to femoral head reduction back into the acetabulum in this positioning. It has been proposed that hip flexion relaxes the tendon, thus classifying it as negligible during reduction. Proving this would also eliminate the iliopsoas muscle as a contributor to reduction, and hence make accounting for it in the dynamic finite element analysis unnecessary.

In order to observe the orientation of the iliopsoas tendon during varying degrees of abduction and flexion, a cadaveric dissection was performed by orthopaedic surgeon Charles T. Price, M.D. Both healthy and dysplastic hips were studied and observations were captured with high definition photography and video. The study aimed to provide insight as to the positioning of the iliopsoas tendon during abduction and flexion, for previously the interaction between the

tendon and the hip joint focused on the neutral position as carried out by Alpert et al. Aside from developmental hip dysplasia, the study could also aid treatments for other disorders such as snapping hip, labral lesions, and iliopsoas impingement.

With the femoral head lying in its correct anatomical location within the acetabulum, 0^o abduction & 0^o flexion, 0^o abduction & 15-20^o flexion, 45^o abduction & 0^o flexion, and 45^o abduction & 15-20^o flexion were all analyzed and the orientation of the iliopsoas tendon noted. For a completely dislocated hip, the 0^o abduction & 0^o flexion, 0^o abduction & 90^o flexion, 0^o abduction & $>90^o$ flexion, and 50^o abduction & 90^o flexion configurations were studied. All configurations were completed with the cadaver in the supine position.

The cadaver analyzed belonged to an 87-year-old female and was provided by the University of Central Florida College of Medicine. The wide Smith-Peterson extended anterior surgical technique exposed the right hip joint with the specimen in the supine position. Initially, the sartorius and rectus femoris were severed and laid back conceding a visual of the joint capsule and iliopsoas tendon. In removing the overlapping muscles from the hip joint, precaution was taken to avoid compromising the surrounding tendons and muscles. Subsequently, the adductor muscles were individually released medially near their points of origin to allow for increased maneuverability during abduction of the cadaver. Upon completing the observations for the healthy hip configurations, the hip capsule was incised circumferentially and the ligamentum teres detached from the femoral head in order to allow for the femur to be manually displaced from the acetabulum. Both of these structures are compromised during hip dislocation and do not contribute to hip joint stability.

For each configuration, three-dimensional computer-aided representations of the human pelvis and femur were constructed from acquired computer tomography (CT) datasets using Mimics software (Materialise Inc, Plymouth, MI). In each model, the femur was abducted and flexed to reflect the configurations analyzed during the dissection. A specific iliopsoas tendon was added to each model configuration using the computer-aided modeling features within the software to accurately depict the varying path of travel to the lesser trochanter by the tendon. The origin of the iliopsoas tendon was taken to be the surface on the pubic bone inferior to the inferior iliac spine as demonstrated by Dostal and Andrews [14]. The computer generated representations present a clearer illustration of the orientation of the iliopsoas tendon and further clarify its position relative to the acetabulum which is otherwise difficult to portray through the dissection photographs.

5.2 Healthy (Non-Dysplastic) Hips

For each healthy hip configuration the femoral head resided within its correct anatomical location within the acetabulum. For this segment of the study the hip joint capsule and the ligamentum teres were still completely intact.

5.2.1 0^o Abduction & 0^o Flexion

In the 0^o abduction, 0^o flexion anatomical arrangement, the iliopsoas tendon kept in constant contact with the hip joint capsule as it wrapped across it anteriorly to insert into the lesser trochanter of the femur. The tension in the tendon left no separation between it and the hip capsule; therefore, tendon retraction and hip capsule exposure would both be improved by

release of the tendon and in many cases required. Figure 5.1 and Figure 5.2 illustrate the orientation of the iliopsoas tendon in this configuration for a non-dysplastic hip.

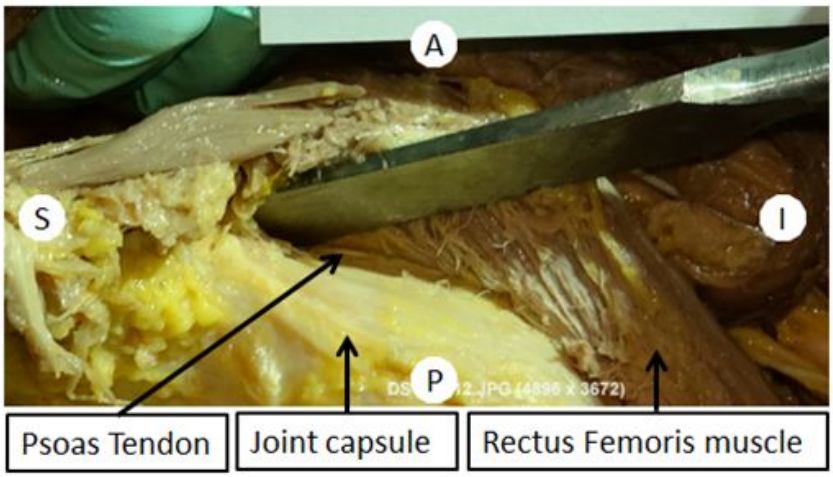

Figure 5.1 Iliopsoas tendon orientation in 0^o abduction and 0^o flexion of a healthy hip

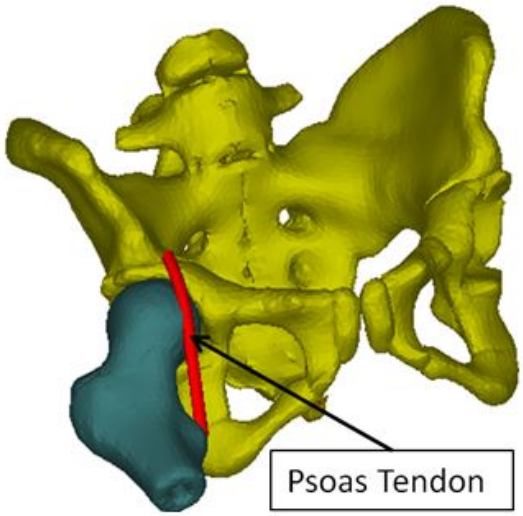

Figure 5.2 Computerized model of the iliopsoas tendon positioning during 0^o abduction & 0^o flexion of a healthy hip

5.2.2 45^{o} Abduction & 0^{o} Flexion

As the femur was manually abducted 45^{o}, the psoas tendon began shifting laterally across the pelvic brim; however, still maintaining continual contact with the hip joint capsule (Figure 5.3, Figure 5.4). The tension present in the tendon during the neutral position remained.

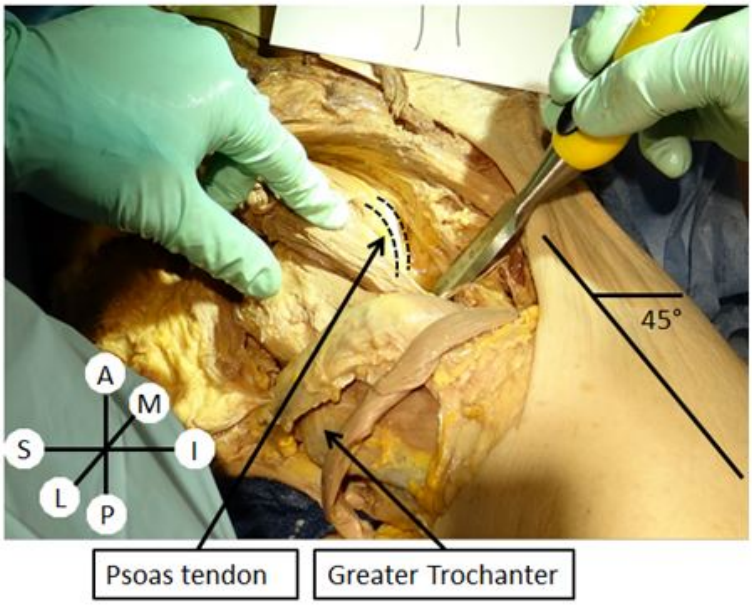

Figure 5.3 Iliopsoas tendon orientation in 45^{o} abduction and 0^{o} flexion of a healthy hip

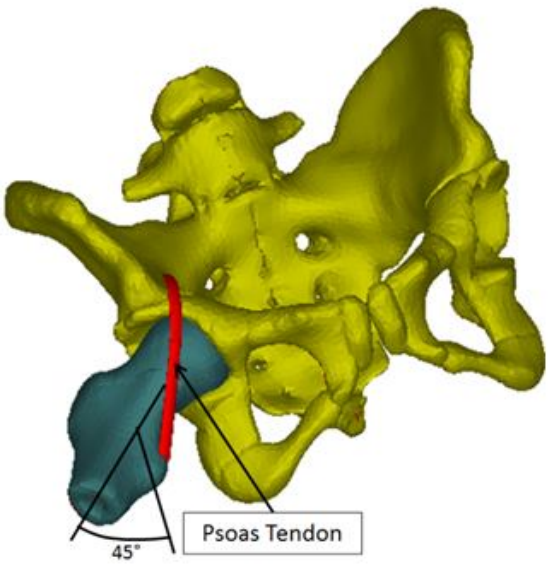

Figure 5.4 Computerized model of iliopsoas tendon positioning during 45^{o} abduction & 0^{o} flexion of a healthy hip

5.2.3 0^{o} Abduction & 15-20^{o} Flexion

The femur was adducted back to its neutral position and then flexed to between 15-20^{o} which was determined visually using a ruler as an angle iron with the dissection table acting as a base to the right angle. Here the iliopsoas tendon became relaxed with no tension present, and separation existed between the tendon and the pelvic brim as well as the anterior capsulolabral complex; hence no interference existed with the joint capsule or femoral head.

5.2.4 45^{o} Abduction & 15-20^{o} Flexion

While maintaining 15-20^{o} flexion and abducting the hip 45^{o} again, the iliopsoas tendon remained relaxed. Upon abduction of the femur, a visible gap formed between the tendon and the capsulolabral complex indicating that any interference in this positioning would be negligible. Additionally, the posteromedial region of the hip joint capsule along with the

adductor muscles were released to allow for the femur to be further flexed to approximately 90^{o}. The tendon exhibited a fully relaxed state in this configuration and would allow for slight retraction without the release of the tendon if necessary.

5.3 Completely Dislocated Hips

To begin observing the iliopsoas tendon for the dislocated configurations, the capsulolabral complex and the ligamentum teres were surgically separted from their respective attachments onto the proximal femur. The femoral head was manually popped out of the acetabulum and placed on the body of the pelvis at the immediate location superior to the acetabular labrum.

5.3.1 0^{o} Abduction & 0^{o} Flexion

In the neutral configuration, the iliopsoas tendon became tense and crossed over the acetabulum, thus blocking the path of reduction for the femoral head (Figure 5.5, Figure 5.6).

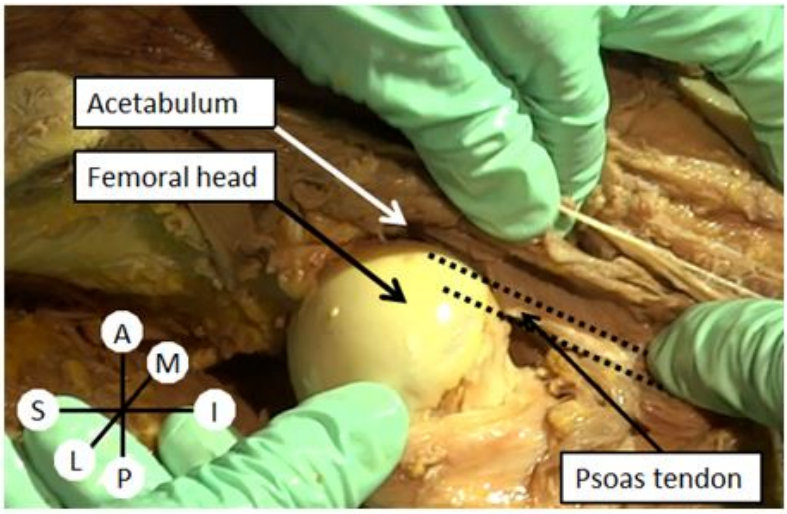

Figure 5.5 Iliopsoas tendon orientation in 0^o abduction and 0^o flexion of a dysplastic hip

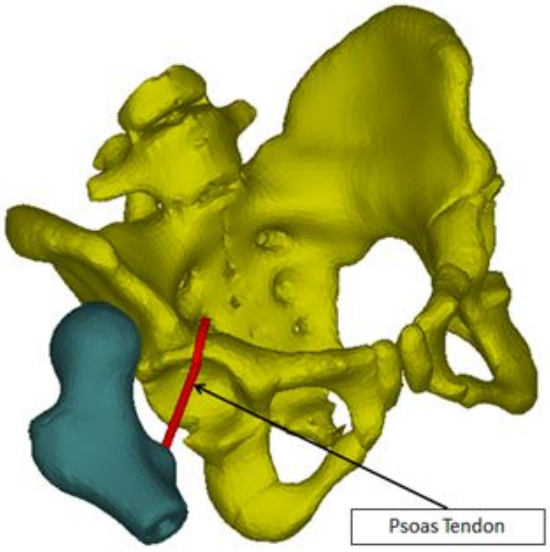

Figure 5.6 Computerized model of iliopsoas tendon orientation during 0^o abduction & 0^o flexion of a dysplastic hip

5.3.2 0^o Abduction & 90^o Flexion

While dislocated, flexion of the femur up to 90^o forced the femoral head to rotate along the acetabular labrum to a more posterior positioning with respect to the acetabulum. During the hip flexion, the tendon began to relax and shifted anteroposterior to the acetabulum allowing for a reduction path. The line of action of the tendon now vectored anterior to both the acetabulum and femoral head as shown in Figure 5.7 and the computer reconstruction in Figure 5.8.

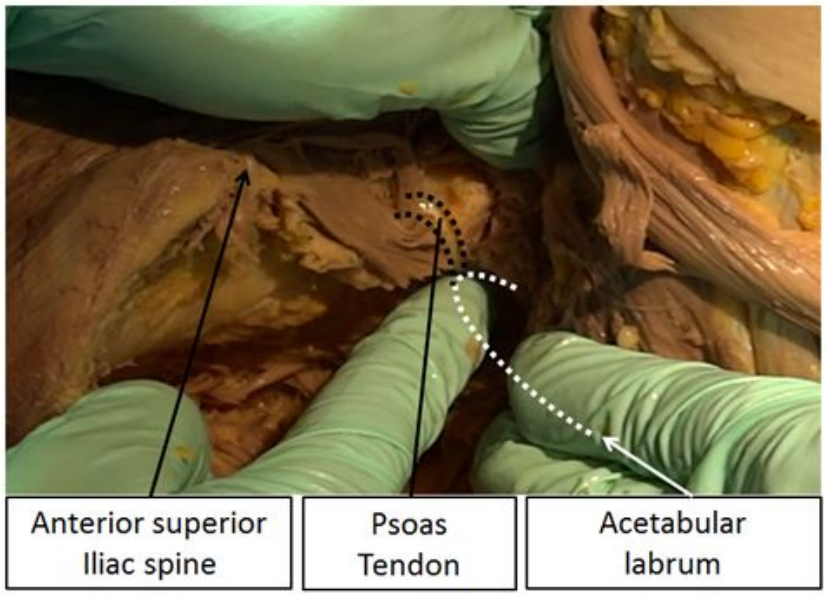

Figure 5.7 Iliopsoas tendon orientation in 0^o abduction and 90^o flexion of a dysplastic hip

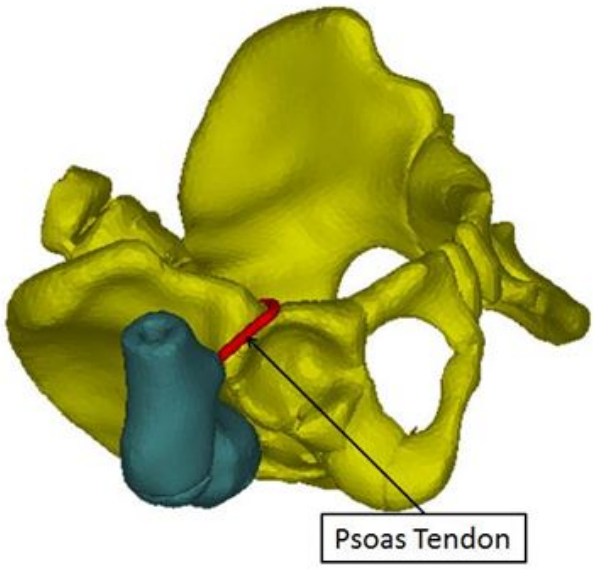

Figure 5.8 Computerized model of iliopsoas tendon positioning during 0^o abduction & 90^o flexion of a dysplastic hip

5.3.3 0^o Abduction & $>90^o$ Flexion

The psoas tendon relaxed further as the degree of flexion increased and the femoral head moved inferiorly along the acetabular lip. In this configuration, also known as hyperflexion, the psoas tendon did not obstruct the acetabulum, and hence would not hinder hip reduction.

5.3.4 50^o Abduction & 90^o Flexion

As hip abduction was implemented with a flexion of 90^o, the psoas tendon remained superior of the acetabulum and the femoral head resided posterosuperior of the acetabular labrum. Although the tendon became slightly taut with hip abduction, this tension was much smaller in comparison to that present when the dislocated hip was in the neutral configuration. The psoas tendon followed a path anterior to the hip capsule, thus eliminating it as an obstruction to hip reduction (Figure 5.9).

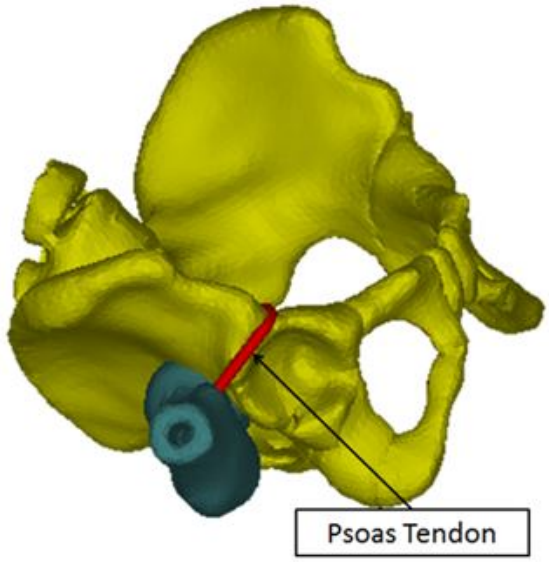

Figure 5.9 Computer model of iliopsoas tendon positioning during 50^{o} abduction & 90^{o} flexion of a dysplastic hip

5.4 Discussion

Based on the observations of the study, it is apparent that the iliopsoas tendon is not an obstruction to hip reduction for a completely dysplastic hip when the hip joint is in flexion. The tendon remains in a relaxed state during flexion irrespective of the degree of abduction and moves laterally when abduction is performed. As the flexion angle increases, the femoral head slides along the circular contour of the acetabular labrum from a position superoposterior of the acetabulum to an inferior location beneath it while the line of action of the iliopsoas tendon shifts anterior and superior of the joint capsule and acetabulum allowing for reduction. When the hip is in the neutral position, however, the tendon compresses onto the joint capsule and hinders reduction. The tension in the tendon increases with an increasing abduction angle when 0^{o} flexion is maintained. It should be noted that in some cases the psoas tendon adheres to the joint

capsule, and thus requires release even in flexion; however, in a study performed by Ishii et al., this condition occurred less than 10% of the time [33]. Nevertheless, this study observed an iliopsoas tendon that was not adherent to the joint capsule.

CHAPTER 6
DISCUSSION

6.1 Improvements on Preliminary Studies

In completing accurate anatomical computer models representative of an infant pelvis and femur, the first step towards completing a dynamic finite element analysis to study the biomechanics of hip dysplasia has been achieved. Preliminary studies on congential hip dysplasia had been accomplished using SolidWorks (Dassault Systèmes Simulia Corp., Providence, RI, USA) where the femur and pelvis were represented by rudimentary solid CAD models (Figure 6.1) [34]. In this simplified model, the solid geometries approximated the surfaces where muscle origins and insertions take place at the pelvis and femur respectively. The femur, conjoined tibia and fibia, and foot were treated as rigid bar elements to obatin a finite element method solution utilizing the FEM software NX Nastran (Siemens PLM Software, Plano, TX, USA). The study analyzed Graf III and Graf IV types of dysplasia simulating each with the hip initially abducted and flexed to match the configuration of the Pavlik harness. A tension function was applied to the linear path of action of each muscle, and passive hip reduction was simulated. Despite its simplified models, the simulation did reveal that correction for subluxated hips using the Pavlik harness is attainable, but for complete dislocation all muscles developed resultant loads that hinder reduction [34].

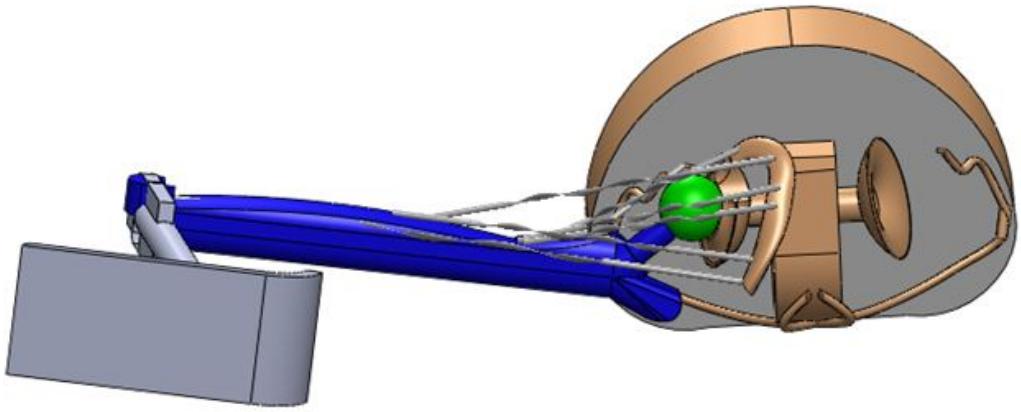

Figure 6.1 Simplified SolidWorks model of an infant hip joint [33]

The SolidWorks model geometry was constructed based on measurements taken from CT and MR images of a 6-month-old which as previously discussed lacks high quality resolution [34]. Furthermore, the most critical regions in studying the biomechanics of the hip joint involve the femoral head and acetabulum along with the muscle origins along the ischium and pubis, all of which are mainly cartilage in an infant and thus translucent in medical imaging. The lack of visible structure for these regions in the images introduces significant error into the measruements upon which the models were based off. The CT-derived models will eliminate these ambigious measurements allowing for a more precise physiological location for the origins and insertion points of the adducting muscles. This increased accuracy will better define the force vectors and possibly affect the force magnitudes, hence altering the overall results.

Additionally, since the SolidWorks model did not encompass a complete anatomical geometry of the pevlis or femur, the unique cartiliginous characteristics of an infant hip joint

could not be applied. The nonhomologous material composition of the infant pelvis and femur has a significant effect on the behavior of the hip during reduction. The segmented anatomical models will improve upon the completely rigid SolidWorks model and provide a more realistic simulation of the mechanisms for hip reduction.

6.2 A Complete Finite Element Model

A tetrahedral volume mesh will be grown for each defined coritcal, cancellous, and cartiliginous region respectivley from these segmented anatomical models using the 3-Matic meshing tools, and subsequently exported into the FEA software Abaqus (Dassault Systèmes Simulia Corp., Providence, RI, USA) in order to perform the simulation (Figure 6.2). Within Abaqus, the pelvis and femur will be assembled, material properties will be assigned to the appropriate volume meshed regions, and the adducting muscles will be simulated in the passive state.

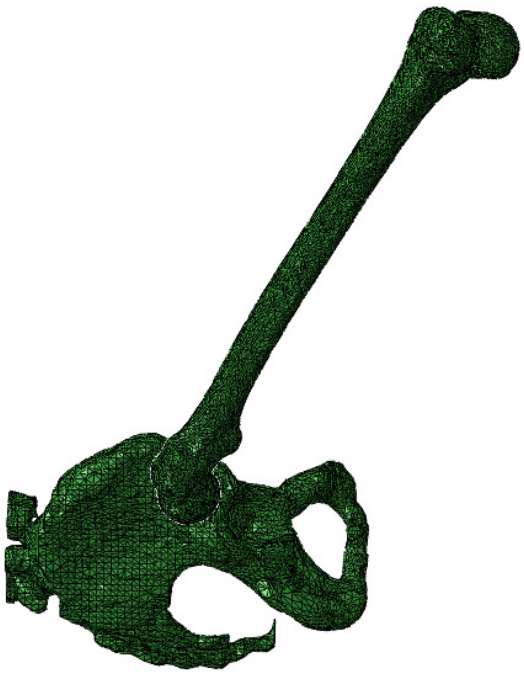

Figure 6.2 Volume meshes of an infant pelvis and femur assembled in Abaqus

In a study on the biomechanics of the hip joint performed by Dostal and Andrews, 20 hip muscles were analyzed using a simplified straight-line approach [18]. The study concluded that the straight-line approach for force generation in a muscle can accuately represent in vivo data despite its conceptual simplicity. Initially, the muscles of interest will be incorporated into the model by defining their points of origins and insertions using this simplified straight-line model (Figure 6.3). These lines of action correlate with the approximate centerline of the muscles. In order to better capture the behavior of the sheet-like shape as well as account for the broad femoral attachment region of the adductor magnus, the simplified model divides the muscle into three distinct components which correspond to the proximal, middle, and distal femoral attachments. Applying a mathematical expression characteristic of the elastic properties for each

specific muscle to its line of action, a simulation can be performed to observe the path of least resistance for hip reduction. This musculoskeletal model will provide a solid baseline to further build upon with additional detail to attain more defined results.

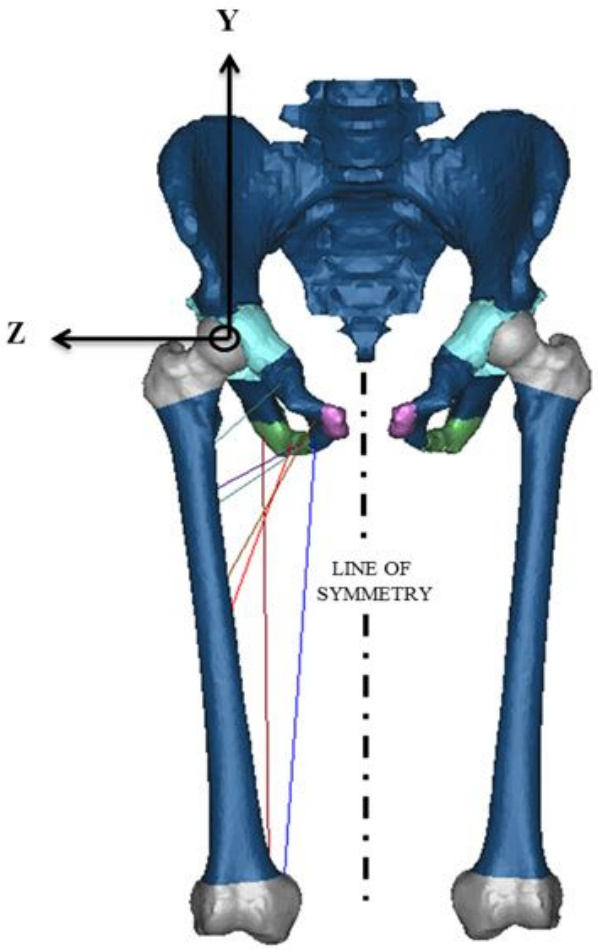

Figure 6.3 Muscle lines of actions applied to hip model

One aspect of this hip model that will be further defined is the muscular models. Future in depth studies will integrate true muscle geometries derived from MRI data images as

demonstrated by Arnold et al [18]. These three-dimensional muscle models will exhibit well defined volumes as well as interfacing surfaces that boundary conditions can then be applied to in order to represent the physiological interactions the muscle may have with underlying and overlying anatomical structures. With the use of a finite element solver, the fully reconstructed musculoskeletal model of the hip joint will yield definitive results .

When the femur and pelvis are assembled within the Abaqus interface they will be oriented to represent the typical orientation of the Pavlik harness treatment which is 80^{o} abduction and 90^{o} flexion with the hip completely dislocated and the femoral head residing in contact with the bony pelvis superoposterior to the acetabular labrum. In regards to the position of the hip joint, this orientation will serve as the intial condition. Based on the preliminary SolidWorks study and documented cases by physicians, one would expect reduction to fail. Validation of this model will permit additional simulations involving variations in abduction and flexion angles. Such analyses could shed light on the most effective abduction and flexion combinations that promote hip reduction in severe cases such as total dislocation.

6.3 Additional Studies

As noted earlier, the success rate of the Pavlik harness is inversely related to age and diminishes significantly after the patient has reached 9 months of age. Papadimitriou et al. documented the use of a modified Hoffman-Daimler to successfully reduce the hip in patients outside of this 9 month age range [35]. The two step method utilizes a flexion harness to promote the reduction process and then an abudction harness is fitted onto the patient for hip remodeling once the abnormality is corrected. This literature finding proposes an alternative

treatment method to the Pavlik harness for patients who were late or misdiagnosed as well as patients afflicted with severe displastic conditions. Using the CT-based models, a case study on the biomechanics of hyperflexion in resolving complete hip dislocation will be performed to further investigate this hypothesis (Figure 6.4).

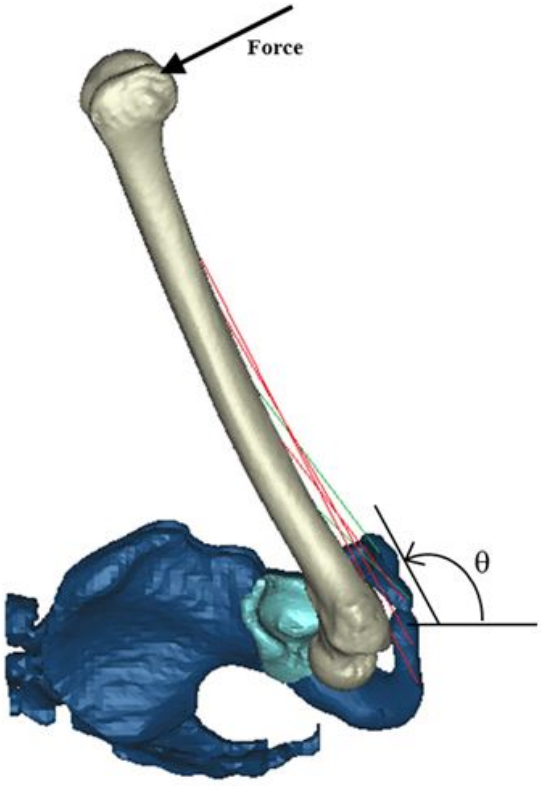

Figure 6.4 Hip model in the hyperflexion configuration

Furthermore, the anteversion (AV) angle of the femur could have a significant affect on the success rate of hip reduction. Varying the femoral AV angle in simulations would lead to even more in depth patient-specific treatments. If varying AV angles were proven to have

distinct optimal abduction and flexion configurations for reduction, physicians would be able to base treatment approaches off of this measurement. Such a study could be completed following the same methods for dynamic finite element analysis but altering the AV angle of the femur model using the design features in 3-Matic prior to export into the FEA software. Femur models with varying AV angles can be observed in Figure 6.5.

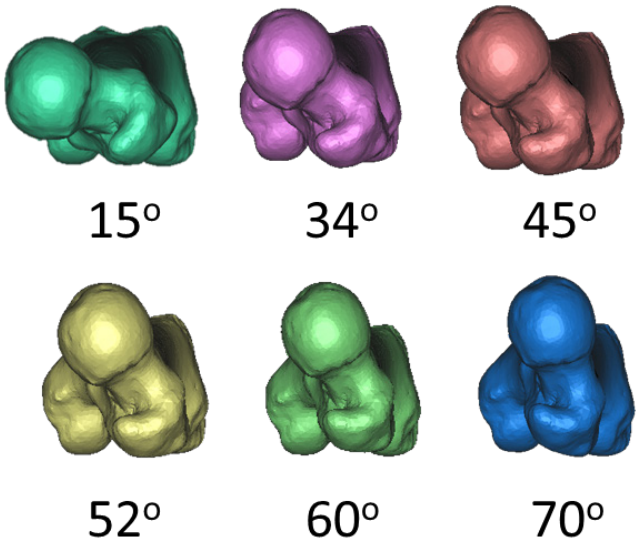

Figure 6.5 Superior view of femur computer models with varying AV angles

CHAPTER 7
CONCLUSIONS

Finite element models derived from CT scans have become a customary and powerful tool for performing analyses on the human anatomy. The workflow allows for the creation of the complex geometry the human body exhibits without the need for CAD modeling. While most methods involving CT-derived anatomical models for FEA purposes extract medical information from a single patient, the low quality resolution present in imaging on infants required multiple patient geometries to be combined in order to construct a complete hip joint of an infant anatomy. Such an aggregate of human data was composed using scaling techniques as well as geometric modifications to yield a solid pelvis and femur model representative of a 10-week-old infant. The natural ossification process of bone occurring during early childhood led to distinguished cartilaginous regions in the acetabulum of the pelvis and the femoral head and epicondyles of the femur. The unique cartilaginous characteristics of the infant hip joint will have a significant effect on the mechanism for hip reduction. In developing the model, the first step in pre-processing was accomplished, leaving generating a mesh, assigning material properties, and applying loads and boundary conditions left in order to perform a dynamic finite element analysis on the hip joint.

As with any FEA, the mechanical properties will need to be accurately assigned for the distinguished material regions segmented in the solid models. In literature, the mechanical properties of both femoral cortical and cancellous bone were inconsistent. After eliminating outlying values from a literature review, the average modulus of elasticity for femoral cancellous bone was found to be 378 MPa with a standard deviation of 29.103 MPa, and the average

modulus of elasticity for femoral cortical bone resulted in 17.66 GPa with a standard deviation of 1.013 GPa. As for the pelvis region, Spears et al. documented the use of 100 MPa for cancellous tissue and 5600 MPa for cortical tissue [24]. Athanasiou et al. recorded an average elastic modulus of 1.186MPa and 1.236MPa for the articulate cartilage of the femoral head and acetabulum respectively [27]. These property values all correspond to an adult hip joint, and hence will need to be either validated for an infant or correlated with age. Another approach would be to develop elastic modulus equations as a function of density as performed by Wirtz et al. [29]. The HU value from CT scans could be applied to determine local densities in which to determine such relations. The only recorded infant mechanical properties for bone tissue found in literature were 10 N/mm^2 for the ultimate-tensile stress, 1.850% for the ultimate tensile strain, and 1012.9 kg/mm^2 for the tangent modulus [30].

In addition to the development of the computerized hip model, the behavior of the iliopsoas tendon and how it effects hip reduction through varying abduction and flexion angles was studied during cadaveric dissection. It was found that during hip flexion the iliopsoas tendon becomes relaxed and allows for a path of reduction for the femoral head even when abducted. In the neutral position, however, the iliopsoas tendon intersects the path of reduction of the femoral head in a dysplastic hip requiring the need for tendon release. This observation holds true for any abduction angle where the hip exhibits 0^o flexion. Since the Pavlik harness constrains the patient in a flexed position, it was concluded that the iliopsoas tendon will not obstruct reduction when using this treatment.

The anatomical models generated in this thesis greatly improve preliminary studies on hip dysplasia involving a primitive SolidWorks CAD model to represent the hip anatomy. The

superior geometrical surfaces of the hip joint provided by the CT-based solid models will allow for increased definition in muscle origins and insertions as well as mass representations. The developed infant hip model will not only mature results regarding developmental hip dysplasia and the Pavlik harness treatment, but will also allow for the exploration of alternative treatments and ultimately patient-specific treatment plans.

The CT-based anatomical computer models create the baseline for any study on the biomechanics of the hip joint involving early childhood development. Not only does it allow for an analysis of different degrees of hip dysplasia with varying flexion and abduction angles, but can also be used to study additional hip abnormalities such as snapping hip, Legg-Calve-Perthes syndrome, or femoroacetabular impingement (FAI).

LIST OF REFERENCES

[1] Institute, I.H.D. Beta International Hip Dysplasia Institute. 2010 [cited 2010 June 1st]; Available from: http://www.hipdysplasia.org/default.aspx.

[2] Weinstein, S.L., S.J. Mubarak, and D.R. Wenger, Developmental Hip Dysplasia and Dislocation Part II. The Journal of Bone and Joint Surgery, 2003. 85(10): p. 2024-2035.

[3] Statistics, N.C.f.H., Centers for Disease Control and Prevention - Births and Natality. 2006.

[4] Michaeli, D.A., S.B. Murphy, and J.A. Hipp, Comparison of predicted and measured contact pressures in normal and dysplastic hips. Medical Engineering & Physics, 1997. 19(2): p. 180-186.

[5] http://upload.wikimedia.org/wikipedia/commons/thumb/0/0f/Skeletpelvis-pubis.jpg/800px-Skeletpelvis-pubis.jpg

[6] Hensinger, Robert N. *Standards in Pediatric Orthopedics: Tables, Charts, and Graphs Illustrating Growth*. New York: Raven, 1986.

[7] M. Samsam, *Functionally Oriented Regional Anatomy,* 1st ed.: Hayden-McNeil, 2011.

[8] http://static.ddmcdn.com/gif/hip-dysplasia-screening.jpg

[9] Clarke, N.M., et al., Real-Time Ultrasound in the diagnosis of congenital dislocation and dysplasia of the Hip. Journal of Bone and joint Surgery, 1985. 67-B(3): p. 406-412.

[10] French, Linda M., and Frederick R. Dietz, Screening of Developmental Dysplasia of the Hip. American Family Physician, 1999. 60(1): p. 177-184.

[11] http://www.hipdysplasia.org/Resources/339/FileRepository/Infant%20Hip%20Dysplasia/ /Treatment%20Methods/Pavlik%20Harness/Pavlik%20Labeled.jpg

[12] Mubarak, S., et al., Pitfalls in the Use of the Pavlik Harness for Treatment of Congenital Dysplasia, Subluxation, and Dislocation of the Hip. The Journal of Bone and Joint Surgery, 1981. 64-A(8): p. 1239-1248.

[13] Rombouts, J. and A. Kaelin, Interior (Obturator) Dislocation of the hip in Neonates. Journal of Bone and joint Surgery, 1992. 74-B: p. 708-710.

[14] Harding, M.G.B., T.H. Harcke, R.J. Bowen, J.T. Guille, and J. Glutting, Management of Dislocated Hips with Pavlik Harness Treatment and Ultrasound Monitoring. Journal of Pediatric Orthopaedics, 1997, 17: p. 189-198

[15] Oonishi, H., Mechanical Analysis of the Human Pelvis and its application to the Artificial Hip Joint - By means of the three dimensional Finite Element Method. Journal of Biomechanics, 1983. 16(6): p. 427-444.

[16] Vaverka, M., et al., Stress and Strain Analysis of the Hip Joint using FEM. Technology and Healthcare, 2006. 14: p. 271-279.

[17] Arnold, Allison S., Silvia Salinas, Deanna J. Asakawa, and Scott L. Delp, Accuracy of Muscle Moment Arms Estimated from MRI-based Musculoskeletal Models of the Lower Extremity. Computer Aided Surgery, 2000. 5: p. 108-119.

[18] Dostal, William F., and James G. Andrews, A Three-dimensional Biomechanical Model of Hip Musculature. Journal of Biomechanics, 1981. 14(11): p.803-12.

[19] Harcke, H. T., Myung S. Lee, Lisa Sinning, Nicholas M.P. Clarke, Patricia F. Borns, and G. D. MacEwen, Ossification Center of the Infant Hip. American Journal of Roentgenology, 1986. 147(2):p. 317-321.

[20] Gray, Henry, and Susan Standring. *Gray's Anatomy: The Anatomical Basis of Clinical Practice*. 39th ed. Edinburgh: Elsevier Churchill Livingstone, 2004.

[21] Brown, Thomas D., and Anthony M. DiGioia III, A Contact-Coupled Finite Element Analysis of the Natural Adult Hip. Journal of Biomechanics, 1984. 17(6): p. 437-448.

[22] Ethier, C. Ross, and Craig A. Simmons. *Introductory Biomechanics From Cells to Organisms*. Cambridge: Cambridge University Press, 2007.

[23] Taylor, M., M.A.R. Freeman, and A.L. Yettram, Cancellous Bone Stresses Surrounding the Femoral Component of a Hip Proshetis: an Elastic-Plastic Finite Element Analysis. Medical Engineering & Physics, 1995. 17(7): p. 544-550.

[24] Taddei, Fulvia, et al., Subject-specific Finite Element Models of Long Bones: An In Vitro Evaluation of the Overall Accuracy. Journal of Biomechanics, 2006. 39: p. 2457-2467.

[25] Spears, Iain R., et al., The Effect of Interfacial Parameters on Cup-bone Relative Micromotions: A Finite Element Investigation. Journal of Biomechanics, 2001. 34: p. 113-120.

[26] Polgár, K., et al., Strain Distribution Within the Human Femur Due to Physiological and Simplified Loading: Finite Element Analysis Using the Muscle Standardized Femur Model. Journal of Engineering in Medicine, 2003. 217(H): p. 173-189.

[27] Rohlmann, A., et al., Finite-element-analysis and Experimental Investigation of Stresses in a Femur. Journal of Biomedical Engineering, 1982. 4(3): p. 241-246.

[28] Athanasiou, K.A., A. Agarwal, and F.J. Dzida, Comparative Study of the Intrinsic Mechanical Properties of the Human Acetabular and Femoral head Cartilage. Journal of Orthopaedic Research, 1994. 12(3): p. 340-349.

[29] Armstrong, C.G., and V.C. Mow, Variations in the Intrinsic Mechanical Properties of Human Articular Cartilage with Age, Degeneration, and Water Content. The Journal of Bone and Joint Surgery, 1982. 64-A(1): p. 88-94.

[30] Wirtz, Dieter C., et al., Critical Evaluation of Known Bone Material Properties to Realize Anisotropic FE-simulation of the Proximal Femur. Journal of Biomechanics, 2000. 33: p. 1325-1330.

[31] Hirsch, C. and F.G. Evans, Studies On Some Physical Properties of Infant Compact Bone. Acta Orthopaedica Scandinavica, 1965. 35(1-4): p. 300-313.

[32] Peng, L., J. Bai, X. Zeng, and Y. Zhou, Comparison of Isotropic and Orthotropic Material Property Assignments on Femoral Finite Element Models Under Two Loading Conditions. Medical Engineering & Physics. 2006, 28: p.227-233.

[33] Ishii, Y., S.L. Weinstein, and I.V.Ponseti, Correlation Between Arthrograms and Operative Findings in Congenital Dislocation of the Hip. Clin Orthop Rel Res, 1980. 153: p.138-145.

[34] Ardila, O., E.A. Divo, F. Moslehy, G.T. Rab, A.J. Kassab, and C.T. Price, Mechanics of Hip Dysplasia Reduction in Infants Using the Pavlik Harness: A Physics-Based Computational Model. Journal of Biomechanics, (in press, accepted, March 2013)

[35] N. G. Papadimitriou, et al., Late-Presenting Developmental Dysplasia of the Hip Treated with the Modified Hoffmann-Daimler Functional Method. Journal of Bone and Joint Surgery. 2007, 89: p. 1258-1268.